AD-A083 570 MANCHESTER UNIV/UNIV OF MANCHESTER INST OF SCIENCE AN--ETC F/G 11/4
MEASUREMENT OF THE THERMAL DIFFUSIVITY OF CARBON/CARBON FIBRE C--ETC(U)
NOV 79 R TAYLOR, R N PROCTER AFOSR-77-3449
UNCLASSIFIED AFOSR-TR-80-0320 NL

1 OF 1
AD A083570

END
DATE FILMED
5-80
DTIC

Manchester Univ. / Univ. of Manchester
Inst. of Science and Technology
(England) Dept. of Metallurgy

UNCLASSIFIED

SECURITY CLASSIFICATION OF THIS PAGE (When Data Entered)

REPORT DOCUMENTATION PAGE	READ INSTRUCTIONS BEFORE COMPLETING FORM
1. REPORT NUMBER AFOSR-TR- 80-0320	2. GOVT ACCESSION NO. AD-A083 570
	3. RECIPIENT'S CATALOG NUMBER 9
4. TITLE (and Subtitle) Measurement of the Thermal Diffusivity of Carbon/Carbon Fibre Composites From 20-3000°C	5. TYPE OF REPORT & PERIOD COVERED INTERIM 30 Sep 77 - 30 Sep 79
	6. PERFORMING ORG. REPORT NUMBER
7. AUTHOR(s) R.Taylor R.N Procter	8. CONTRACT OR GRANT NUMBER(s) AFOSR-77-3449
9. PERFORMING ORGANIZATION NAME AND ADDRESS Department of Metallurgy University of Manchester/UMIST, Manchester, England	10. PROGRAM ELEMENT, PROJECT, TASK AREA & WORK UNIT NUMBERS 2308/B1 61102F
11. CONTROLLING OFFICE NAME AND ADDRESS AIR FORCE OFFICE OF SCIENTIFIC RESEARCH/NA BUILDING 410 BOLLING AFB, DC 20332	12. REPORT DATE November 1979
	13. NUMBER OF PAGES 66
14. MONITORING AGENCY NAME & ADDRESS (if different from Controlling Office)	15. SECURITY CLASS. (of this report) UNCLASSIFIED
	15a. DECLASSIFICATION/DOWNGRADING SCHEDULE

16. DISTRIBUTION STATEMENT (of this Report)

Approved for public release; distribution unlimited.

17. DISTRIBUTION STATEMENT (of the abstract entered in Block 20, if different from Report)

18. SUPPLEMENTARY NOTES

19. KEY WORDS (Continue on reverse side if necessary and identify by block number)

THERMAL DIFFUSIVITY,
CARBON FIBER CARBON COMPOSITES
LASER PULSE METHOD
HIGH TEMPERATURES.

20. ABSTRACT (Continue on reverse side if necessary and identify by block number)

Thermal diffusivity measurements from 300-3000K have been made on the following materials using the laser pulse method: (a) 3-D carbon fiber carbon composites types 'A' and 'B' made using Fiber "F" material; (b) 1-D carbon fiber composite; (c) the matrix material used in their fabrication. Thermal conductivity has been calculated from these results and a model of composite conductivity presented.

DD FORM 1 JAN 73 1473 EDITION OF 1 NOV 65 IS OBSOLETE

UNCLASSIFIED

GRANT NUMBER AFOSR-77-3[illegible]-9

MEASUREMENT OF THE THERMAL DIFFUSIVITY OF CARBON/CARBON FIBRE COMPOSITES FROM 20-3000°C.

Roy Taylor and Rob Procter
Department of Metallurgy
University of Manchester/UMIST
Grosvenor Street
Manchester
England

November 1979

Interim Scientific Report 30 September 1977 - 30 September 1979

Approved for public release: distribution unlimited

Prepared for

A.F.O.S.R.
BUILDING 410
BOLLING A.F.B.
WASHINGTON D.C. 20332

and EUROPEAN OFFICE OF AEROSPACE RESEARCH AND DEVELOPMENT
LONDON
ENGLAND

and AIR-FORCE MATERIALS LABORATORY
WRIGHT PATTERSON AIR FORCE BASE
OHIO 45433

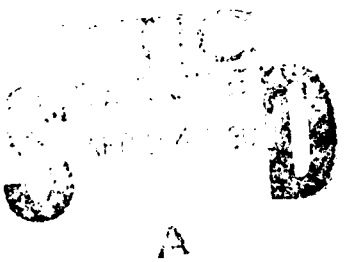

A

Contents

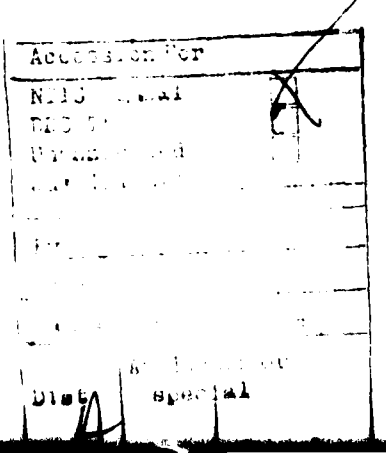

List of Figures

List of Tables

1. INTRODUCTION

The thermal properties of three-dimensional carbon fibre/carbon composites (CFCC), have been investigated over the temperature range 300-3000K.

The first stage of the investigation has been to characterise the thermal conductivity of two different 3D CFCC materials over a temperature range of 300 to 3000K. To achieve this, the thermal diffusivity has been measured using the laser pulse technique[1,2]. This data has then been converted to thermal conductivity using the expression:

$$\lambda = \alpha \rho c_p \qquad (1)$$

where λ is the thermal conductivity (w/cmK), α is the diffusivity (cm^2/scc), ρ is the density ($grms/cm^3$) and c_p is the specific heat (J/gmK).

The structure of the CFCC materials is such that it is necessary to measure diffusivity along two axes to fully characterise their properties.

In parallel with the experimental work, a complementary aim of the investigation has been to model the CFCC thermal conductivity in terms of the properties of its constituents. Accordingly, samples of the matrix material and a 1-dimensional composite were obtained from the Air Force Materials Laboratory (AFML), Wright-Patterson Air Force Base, and these were also measured.

Nominally, the CFCC consists of two distinct phases only; carbon fibre yarns and a carbon matrix material. A consequence of processing procedures however is that an accurate description of the finished composite is more complex. In the absence of accurately quantifiable information on in-situ constituent properties, a somewhat simpler modelling approach has been adopted.

2. DESCRIPTION OF MATERIALS

Material 'A' is a 3-D orthogonal CFCC. The carbon fibres are formed into yarns of 1440 filaments and two such yarns form the fibre reinforcement in each of the X and Y axis. The Z axis reinforcement is composed of three yarns. A unit cell of material 'A' is shown in Figure 1.

Material 'B' is similarly a 3-D composite, but in this case the yarns nominally are not orthogonal. The X and Y yarns are woven in an 8-harness satin weave to form a reinforcement plane which is pierced by the Z yarns (fine weave pierced fabric, FWPF). This type of construction is shown in Figure 2.

The basic properties of materials 'A' and 'B' are listed in Table 1.

The manufacture of a typical 3-D CFCC begins with the construction of a fibre preform. According to current standard processing procedures, the preform is then stiffened by carbon vapour deposition (CVD). The reinforced preform is then densified by impregnation with pitch material at high pressure ($\sim$15000 p.s.i.). After carbonisation at 650^{o}C, the whole composite is graphitised at 2700^{o}C and this impregnation and densification process is typically repeated five times.

The aim of processing is to impregnate the fibre bundles and fill the crossover pockets and other voids with graphitic matrix material.

The properties of fibre and matrix are given in Table 1.

To assist modelling, the following additional specimens were provided by AFML.

1. A 1-D CFCC, nominally processed in the same manner as the 3-D composites. Its properties are given in Table 1.
2. Specimens of the carbon fibre used in all composites.
3. A specimen comprised of graphitised matrix only.

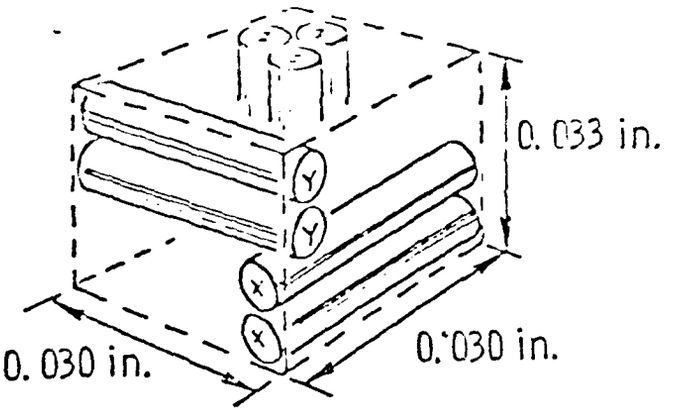

3D ORTHOGONAL
(223)

Figure 1

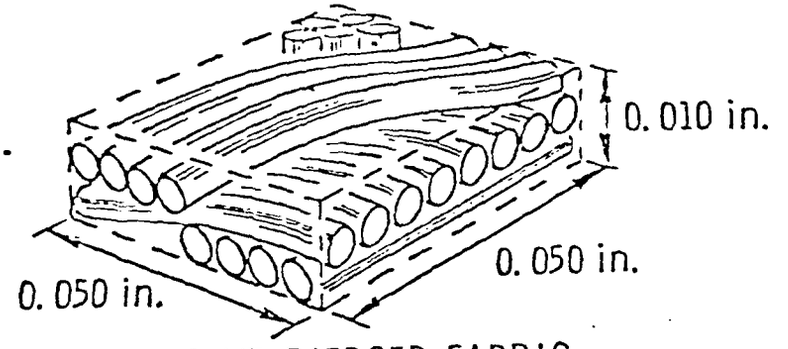

FINE WEAVE PIERCED FABRIC
(FWPF)

Figure 2

	Composite "A"	Composite "B"	Matrix Graphite	1-Dimensional Composite
Bulk density $g.cm^{-3}$	1.883	1.917	1.36	1.915
Open porosity %	6.1	5.95	-	-
Fibre volume fraction X and Y axes	0.13	-	N/A	-
Fibre volume fraction Z axis	0.22	0.132	N/A	-
Thread count yarns/in. X and Y axis	N/A	30	N/A	N/A
Filaments/End X and Y axis	N/A	1400	N/A	N/A
Fibre cross-section	Crenulated	Crenulated	N/A	Crenulated
Fibre bulk density $g\ cm^{-3}$	1.66	1.66	N/A	1.66
Fibre diameter µm	6.50	6.50	N/A	6.50
Filaments per yarn	1440	1440	N/A	1440

Table 1

Materials Specification

3. SAMPLE PREPARATION

Samples of 6.35 mm diameter were cored from each material billet provided. The axial orientation of the samples was chosen to reflect the anisotropic nature of the CFCC materials.

In the case of the matrix material, samples were cored from two orthogonal directions to verify the isotropy of the material.

Sample data is given in Table 2.

Density measurements were made using a liquid densitometer and reveal only minor density variations between samples. Bulk densities are in general 2-5% lower.

4. FLASH DIFFUSIVITY MEASUREMENT TECHNIQUES.

The UMIST apparatus has been described in detail in a number of publications (e.g. 1,3) and will only be briefly summarised here.

The sample front face temperature is instantaneously raised and the subsequent rear face temperature transient recorded.

Thermal diffusivity is calculated from;

$$\alpha = \frac{w}{\pi^2} \frac{L^2}{t_x} \qquad (2)$$

where L is the sample length, t_x ($o<x<1$) is the time for the rear face to reach a given fraction x of its maximum temperature and w/π^2 is a constant whose value depends upon x. The usual choice of x is 0.5 whence $w/\pi^2 = 0.139$.

Since it is unnecessary to measure either absolute or relative temperatures with this technique, its potential accuracy, particularly for high temperature application, is better than conventional thermal conductivity measurement methods, which rely on absolute measurements of a temperature gradient.

Composite Type and Axis	Sample No.	Length cm	Density gm/cm^3
CFCC 'A' X axis	1	0.242	1.926
" " " "	2	0.242	1.920
CFCC 'A' Z axis	1	0.399	1.916
" " " "	2	0.398	1.887
" " " "	3	0.298	1.919
" " " "	4	0.301	1.925
CFCC 'B' X axis	1	0.439	1.95
" " " "	2	0.439	1.94
CFCC 'B' Z axis	1	0.338	1.936
" " " "	2	0.336	1.931
" " " "	3	0.338	1.928
1-D CFCC // axis	1	0.454	1.910
" " "	2	0.458	1.905
1-D CFCC TF axis	1	0.1995	1.900
" " " "	2	0.152	1.897
" " " "	3	0.1992	1.910
Bulk Matrix	1	0.297	1.369
" "	2	0.3005	1.389

Table 2

Sample Information

The present UMIST diffusivity facility employs a 100 J ruby laser to heat the specimen front face and the rear face transient is digitally logged under computer control. To minimise the influence of finite pulse time on the rear face transient and to provide correction for heat losses[1,4] it is desirable to restrict the range of $t_{0.5}$ to 25 msec < $t_{0.5}$ < 200 msec. This is generally possible by judicious choice of sample length.

Suitable programming enables the computation of $t_{0.5}$ to a precision better than 100 microseconds including correction for finite pulse time (5) where necessary. The ratio of transient amplitude at either $5t_{0.5}$ or $10t_{0.5}$ to that at $t_{0.5}$ is then determined and from this information heat loss is evaluated and w/π^2 calculated [4]. Finally, the sample length is corrected for thermal expansion.

5. EXPERIMENTAL PROCEDURE

Diffusivity measurements were carried out on all the materials detailed in Section 2 over a temperature range of 300 to ∿3000K. The extent of this temperature range made it necessary to make the measurements in four distinct sub-ranges, chosen to accommodate the conditions obtaining;

(a) 300-700K: The use of an infra-red (IR) detector with extended long wavelength response or a thermocouple in intimate contact with the sample rear face is required. The former was chosen (InSb detector, liquid nitrogen cooled, cut-off wavelength 5.5 μm) since an optical detector 'sees' an area weighted temperature whereas a thermocouple only senses the temperature at the point of contact. Given the heterogenous nature of most of the samples, the choice was obvious [2].

The accuracy of some measurements made in this range has fallen below that normally achieved with the technique. This has been due to two principal factors 1) Low frequency detector noise resulting from detector temperature fluctuations as the liquid nitrogen coolant slowly boils; 2)

Degredation of signal-to-noise ratio (S/N) at low temperatures. The latter has often been exacerbated by the condition that $t_{0.5}>25$ msec. In high diffusivity samples this requires a long sample, leading to a reduction in the magnitude of the rear face temperature transient and hence in S/N.

(b) 500-1500K: At temperatures of 500K and above it was practical to use a more robust (and cheaper) PbS detector (cut-off wavelength 3.0 μm).

(c) 1200-2300K: For temperatures > 1200K, ambient temperature thermocouple replaced by optical pyrometer.

(d) 2000-3000K: In the preceding temperature ranges, a vacuum ($<1 \times 10^{-4}$ torr) was sufficient to protect the samples. Above 2300K, however, the vapour pressure of graphite increases to such an extent that it is necessary to suppress evaporation by using an inert atmosphere (helium) at about 20 lb/in^2 pressure.

The derivation of thermal conductivity from diffusivity is straight forward provided that accurate specific heat data is available. Used throughout is a least squares fit of specific heat data obtained from two sources (see figure 3). These comprise measurements of POCO graphite (350-1000K) and CFCC 'A' itself (1500-3000K) made by Taylor and Cezairliyan respectively[6]. The least squares function is a 5th order polynomial:

$$c_p = -5.944\times10^{-1} + 5.5076\times10^{-3}T - 4.9454\times10^{-6}T^2 + 2.3389\times10^{-9}T^3 - 5.5749\times10^{-13}T^4 + 5.3241\times10^{-17}T^5 \qquad (3)$$

In addition, AFML thermal expansion data has been used to correct for sample length and density changes with temperature[7].

Specimens used for microstructural investigation were prepared by firstly grinding and polishing down to $\frac{1}{4}$ μm. This was followed by etching for 10-15 minutes in a hot solution of potassium dichromate in phosphoric acid[8]. Finally, the specimens were lightly sputtered with gold for improved electron microscope resolution.

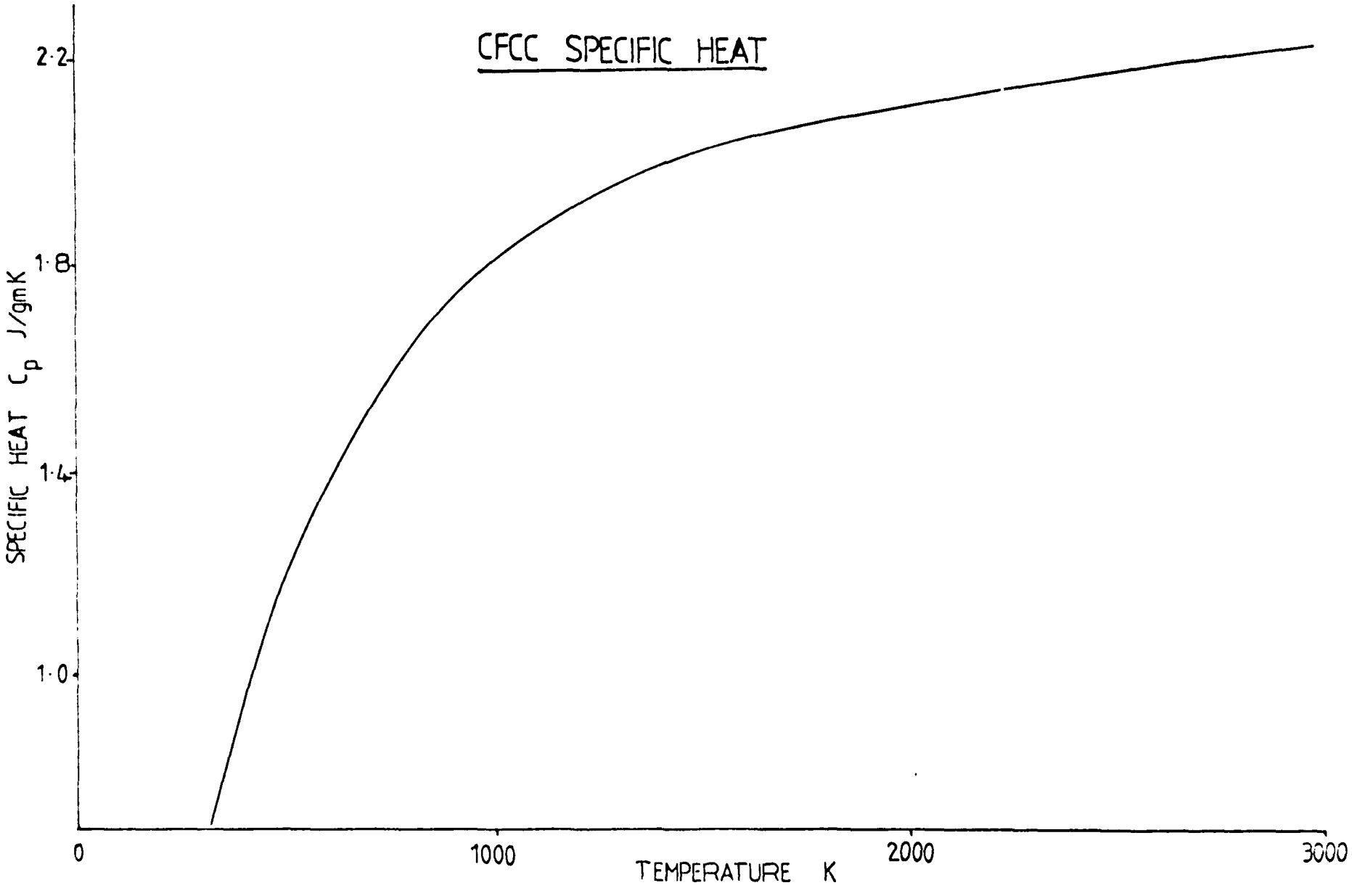
CFCC SPECIFIC HEAT
2·2
1·8
1·4
1·0
SPECIFIC HEAT C_p J/gmK
0
1000
2000
3000
TEMPERATURE K

FIGURE 3

6. EXPERIMENTAL RESULTS

(A) 3-D Composite 'A'

(i) X Axis

The diffusivity of two X axis samples was measured over the complete temperature range. The results are shown in Figure 4. They provide an excellent agreement with AFML flash diffusivity data,[6] also shown, which was obtained from a CFCC similar to 'A'.

Figure 5 shows the X axis conductivity together with directly measured data obtained from different billets of 'A' type material by the comparative rod method[6]. The direct method conductivity is higher at low temperatures, and this may simply be a product of inter-billet variations. However, Taylor and Lee[2] and Minges[9] have observed similar discrepancies between direct and diffusivity-derived conductivity.

There is no systematic difference in the properties of the two samples and this is shown more clearly in Figure 6 which is a plot of % deviation from the least squares function. A number of different functions were tried and for the whole temperature range the best was found to be a fourth order polynomial. The coefficients and rms error are given in Table 3.

(ii) Z Axis

Figure 7 shows the diffusivity of four samples, again compared with diffusivity data from a material similar to composite 'A'[6]. As in the previous case, the agreement of the diffusivity data is good.

Figure 8 shows the resultant conductivity values with comparative rod data for comparison[6]. As before, the latter data is higher. Billet variations or, as Taylor and Lee[2] imply, differences in measurement method may be responsible. In this case, however, it seems appropriate to question the validity of the low temperature specific heat data. Over a temperature range of 350-1000K this relies entirely on the specific heat of POCO graphite,

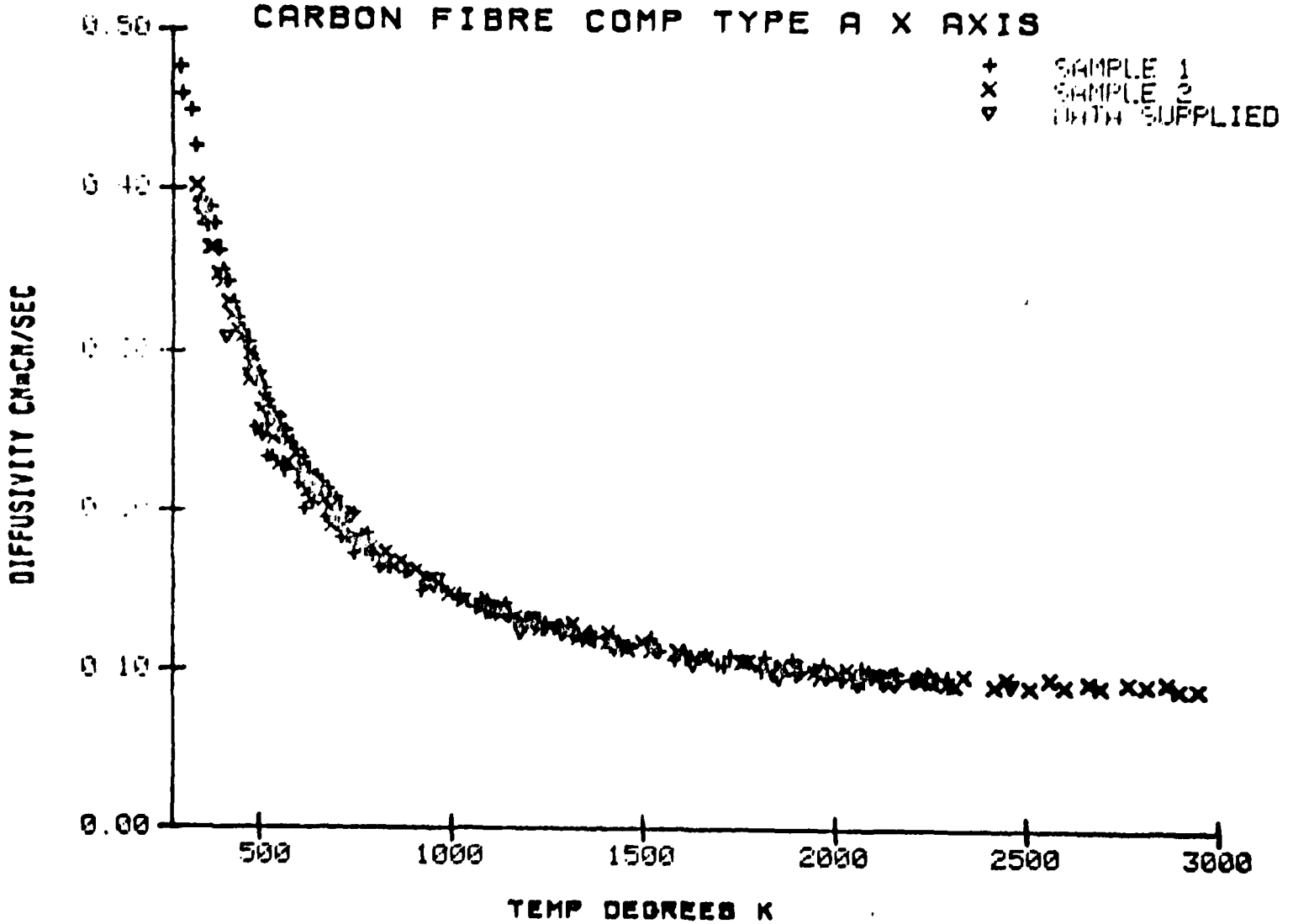
CARBON FIBRE COMP TYPE A X AXIS
SAMPLE 1
SAMPLE 2
DATA SUPPLIED
0.50
0.40
0.30
0.20
0.10
0.00
DIFFUSIVITY CM=CM/SEC
500
1000
1500
2000
2500
3000
TEMP DEGREES K

Figure 4

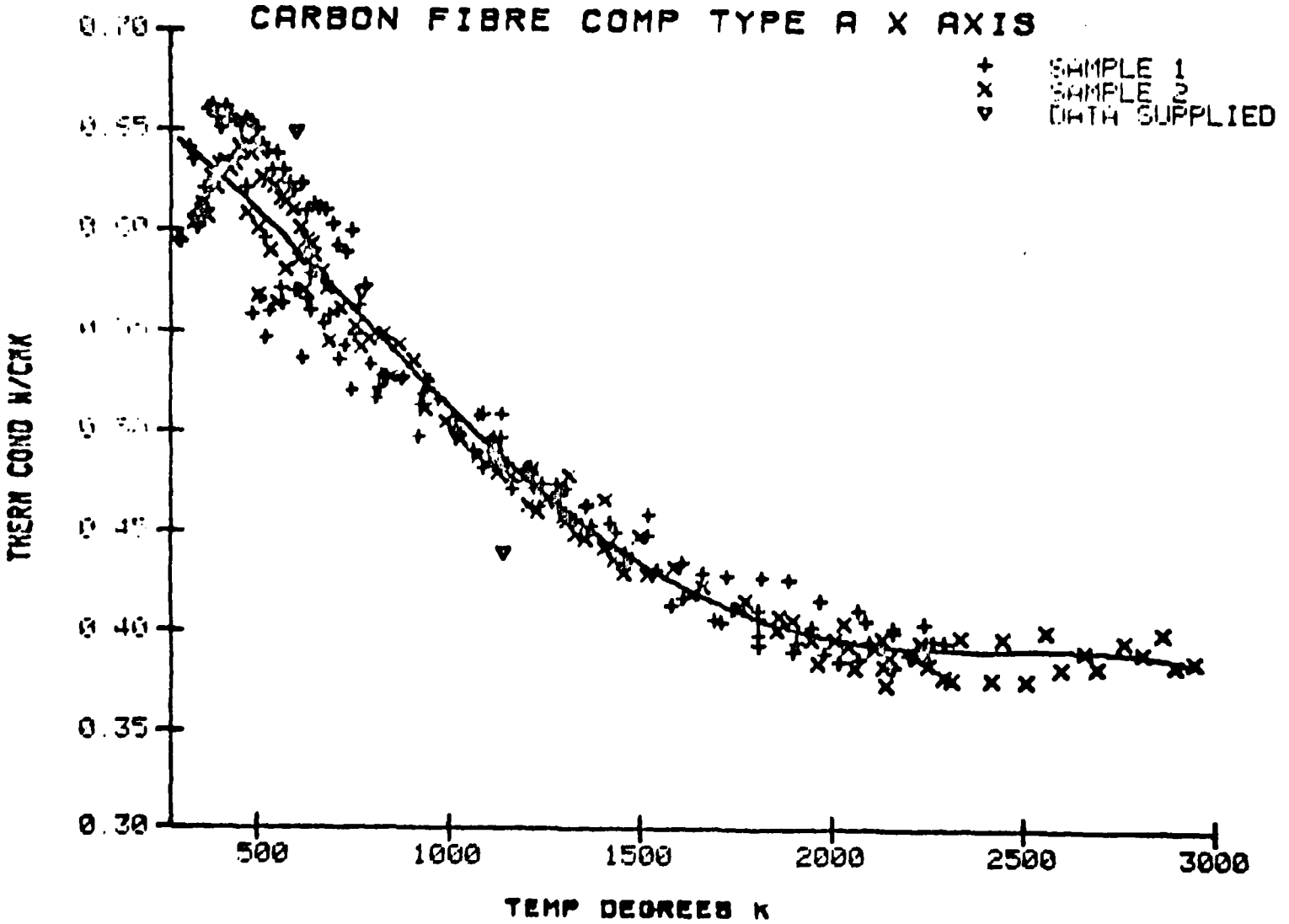
CARBON FIBRE COMP TYPE A X AXIS
SAMPLE 1
SAMPLE 2
DATA SUPPLIED
THERM COND W/CMK
0.70
0.55
0.40
0.35
0.30
500
1000
1500
2000
2500
3000
TEMP DEGREES K

Figure 5

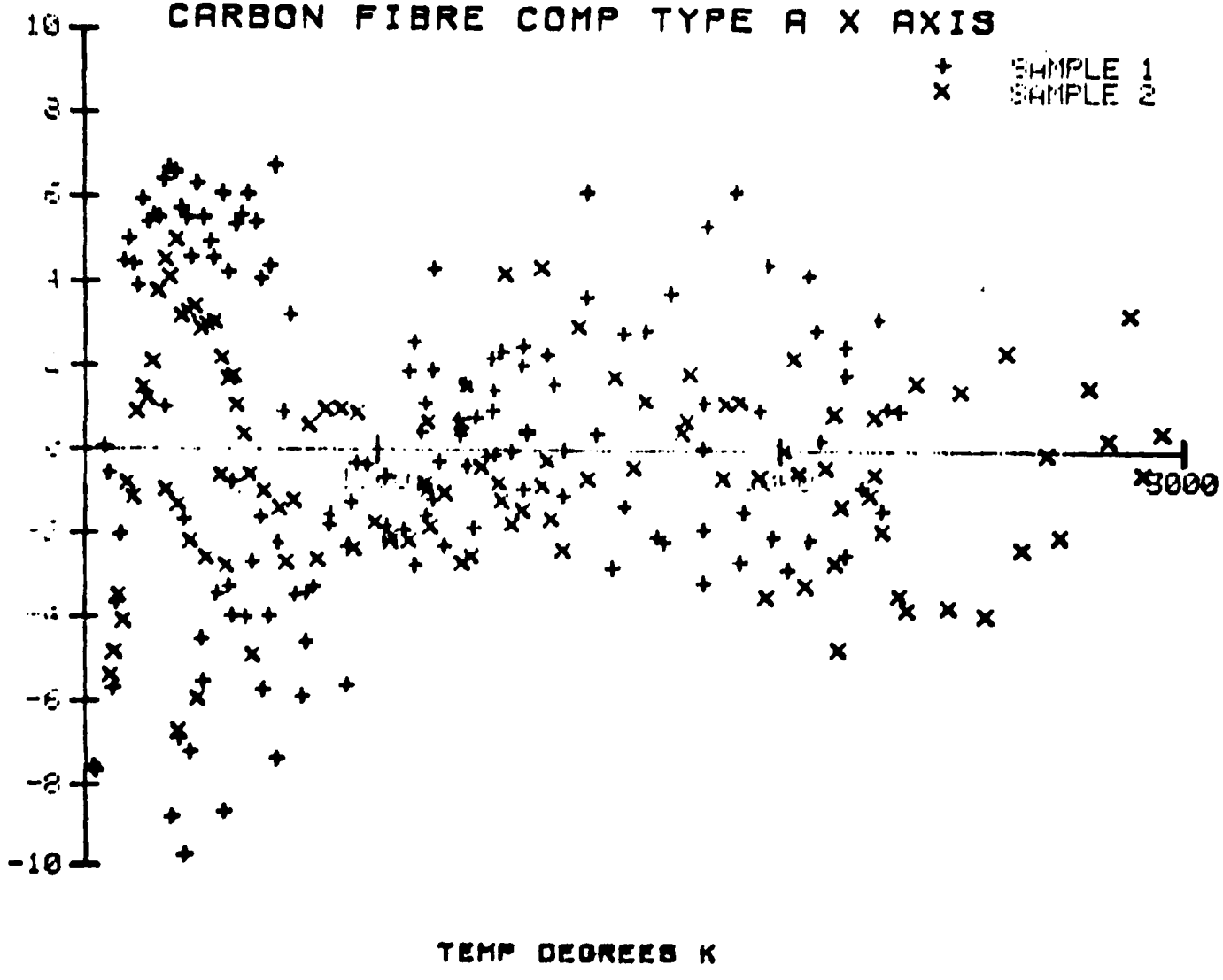
CARBON FIBRE COMP TYPE A X AXIS
SAMPLE 1
SAMPLE 2
10
8
6
4
2
0
-6
-8
-10
3000
% DEVIATION FROM L.SQ. FIT
TEMP DEGREES K

Figure 6

Composite Type and Axis	Coefficients						% RMS Error
	Polynomial Order	T^0	T^1	T^2	T^3	T^4	
CFCC 'A' X axis	4	0.67531	-5.2149×10^{-5}	-2.1528×10^{-7}	1.2428×10^{-10}	-1.921×10^{-14}	3.6
CFCC 'A' Z axis	3	1.0463	-3.9355×10^{-4}	6.4192×10^{-8}	2.2071×10^{-12}	-	3.3
CFCC 'B' X axis	4	1.7611	-1.4727×10^{-3}	7.6701×10^{-7}	-1.8815×10^{-10}	1.7153×10^{-14}	4.3
CFCC 'B' Z axis	4	0.66092	2.0294×10^{-5}	-3.5184×10^{-7}	2.0619×10^{-10}	-3.3782×10^{-14}	4.2
1-D CFCC axis	4	4.1192	-2.9682×10^{-3}	1.1770×10^{-6}	-2.1011×10^{-10}	1.0583×10^{-14}	3.8
1-D CFCC TF axis	4	0.27302	6.6837×10^{-5}	-2.1870×10^{-7}	1.1960×10^{-10}	-2.0259×10^{-14}	3.7
Bulk Matrix	4	0.9020	-1.2206×10^{-4}	-3.9952×10^{-7}	2.4646×10^{-10}	-4.1589×10^{-14}	4.6

Table 3

Least Square Fit Conductivity Functions.

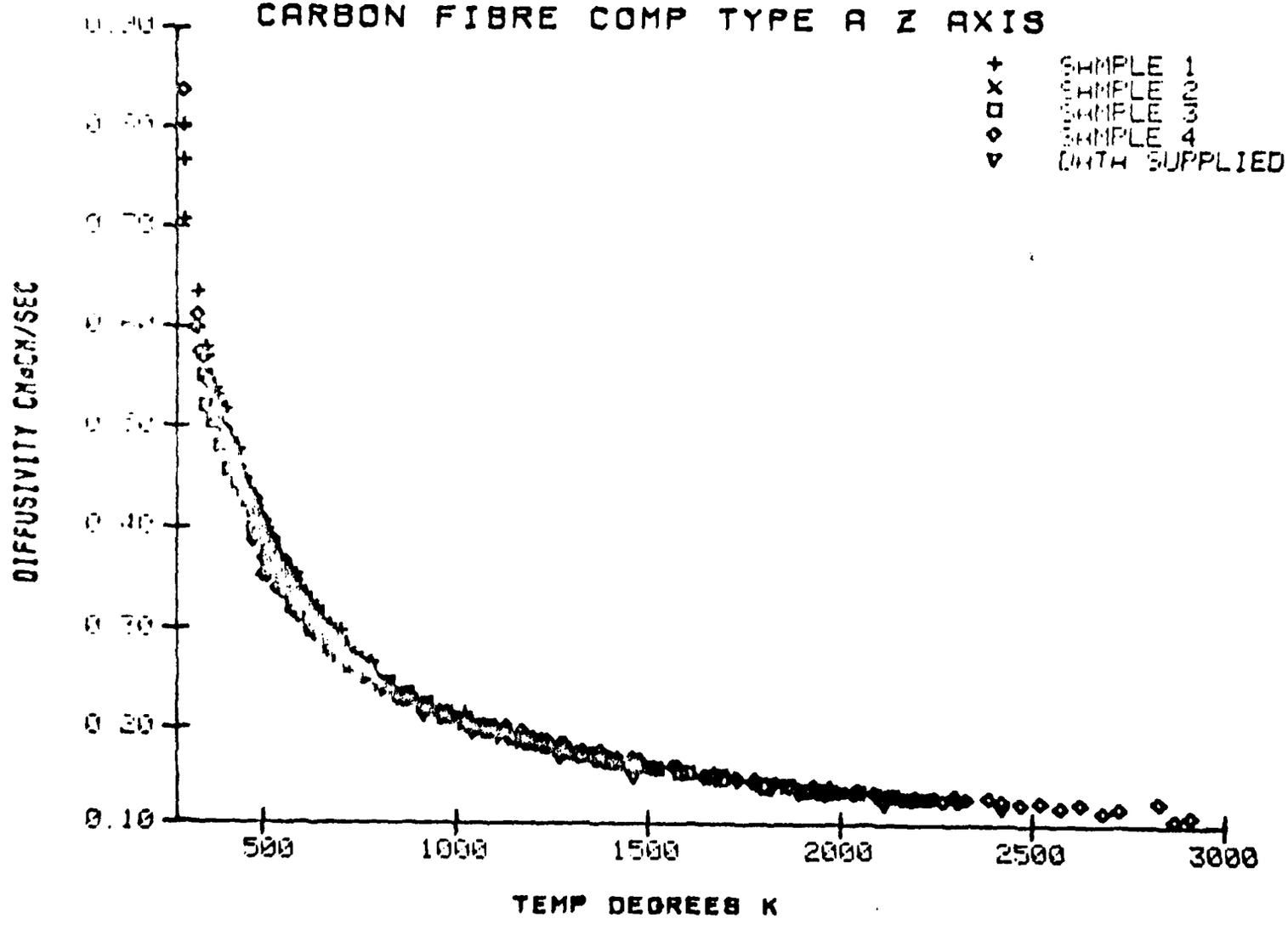
CARBON FIBRE COMP TYPE A Z AXIS
SAMPLE 1
SAMPLE 2
SAMPLE 3
SAMPLE 4
DATA SUPPLIED
DIFFUSIVITY CM*CM/SEC
0.10
0.30
0.40
500
1000
1500
2000
2500
3000
TEMP DEGREES K

Figure 7

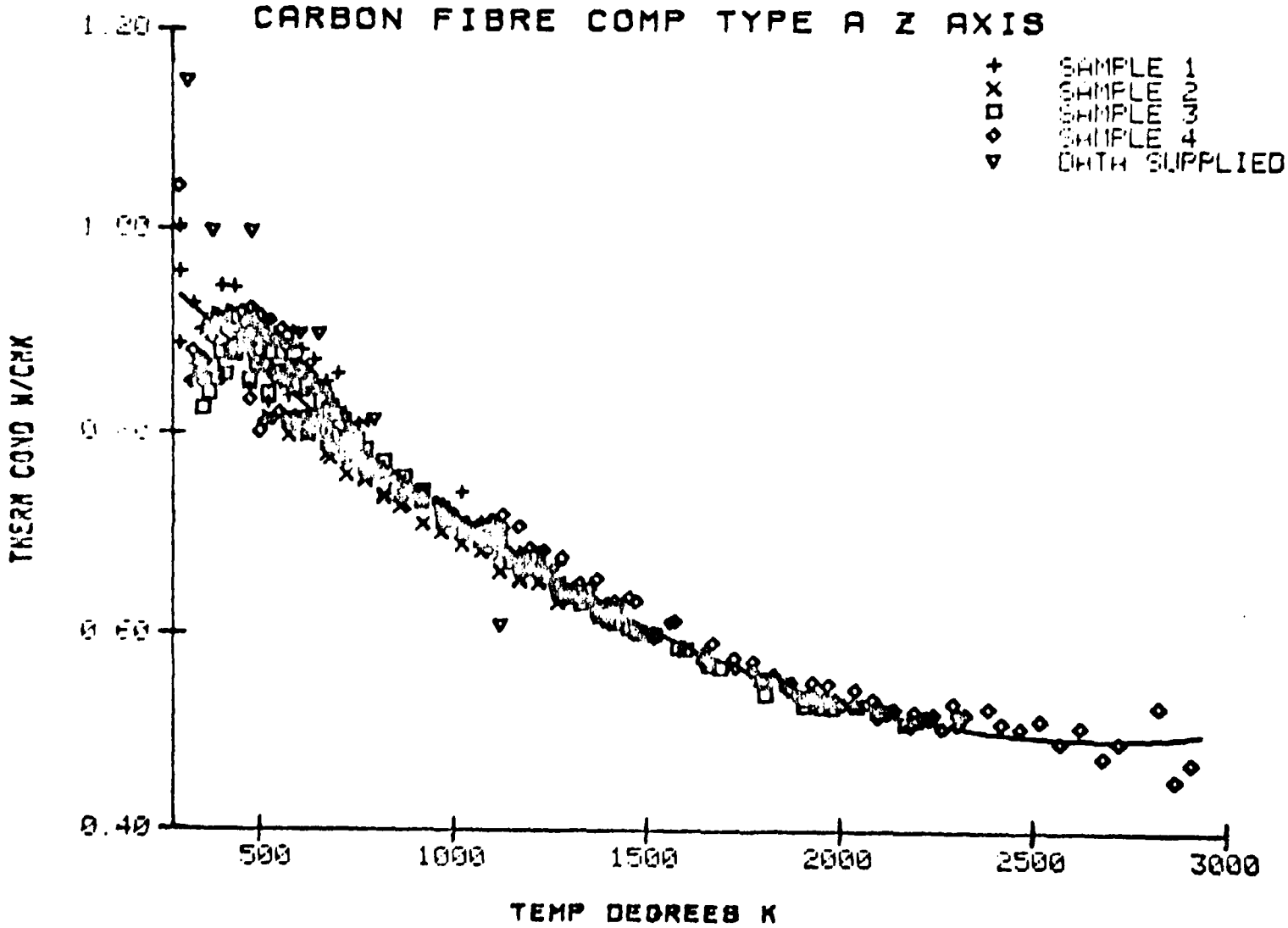
CARBON FIBRE COMP TYPE A Z AXIS
SAMPLE 1
SAMPLE 2
SAMPLE 3
SAMPLE 4
OHTH SUPPLIED
1.20
1.00
0.80
0.60
0.40
THERM COND W/CMK
500
1000
1500
2000
2500
3000
TEMP DEGREES K

Figure 8

whereas there is evidence that the specific heat of fibre 'F' alone is 3 % higher at 300K[2]. The law of mixtures would suggest that the composite 'C' value should lie between these two limits.

Figure 9 shows the data deviation plot for the least squares function given in Table 3. A systematic relationship between deviation and sample can be seen which may be partly, but not completely, explained by differences in sample density (see Table 2).

(B) 3-D Composite 'B'

(i) X Axis

Diffusivity data and derived conductivity values of two X axis samples are shown in Figures 10 and 11 respectively. No comparative diffusivity data is available. However, comparative rod conductivity data[6], from a different billet, shows excellent agreement.

Figure 12 shows the deviation from the least squares fit.

(ii) Z Axis

Diffusivity and conductivity results from three samples are shown in Figures 13 and 14 respectively. Comparative rod data[6], again from a different billet, is higher by a factor of 20-25% over most of the temperature range.

Figure 15 shows that deviation from the least squares fit is broadly sample dependent. Differences in sample densities are insignificant.

(C) Matrix Material

Diffusivity and conductivity results from two bulk matrix samples are shown in Figures 16 and 17 respectively.

The samples were cut orthogonally to determine the degree of anisotropy, if any. The data indicate an essentially isotropic material.

The high porosity of the bulk matrix (~40%) contrasts with the high density of the composites and, by inference, with the low porosity of the

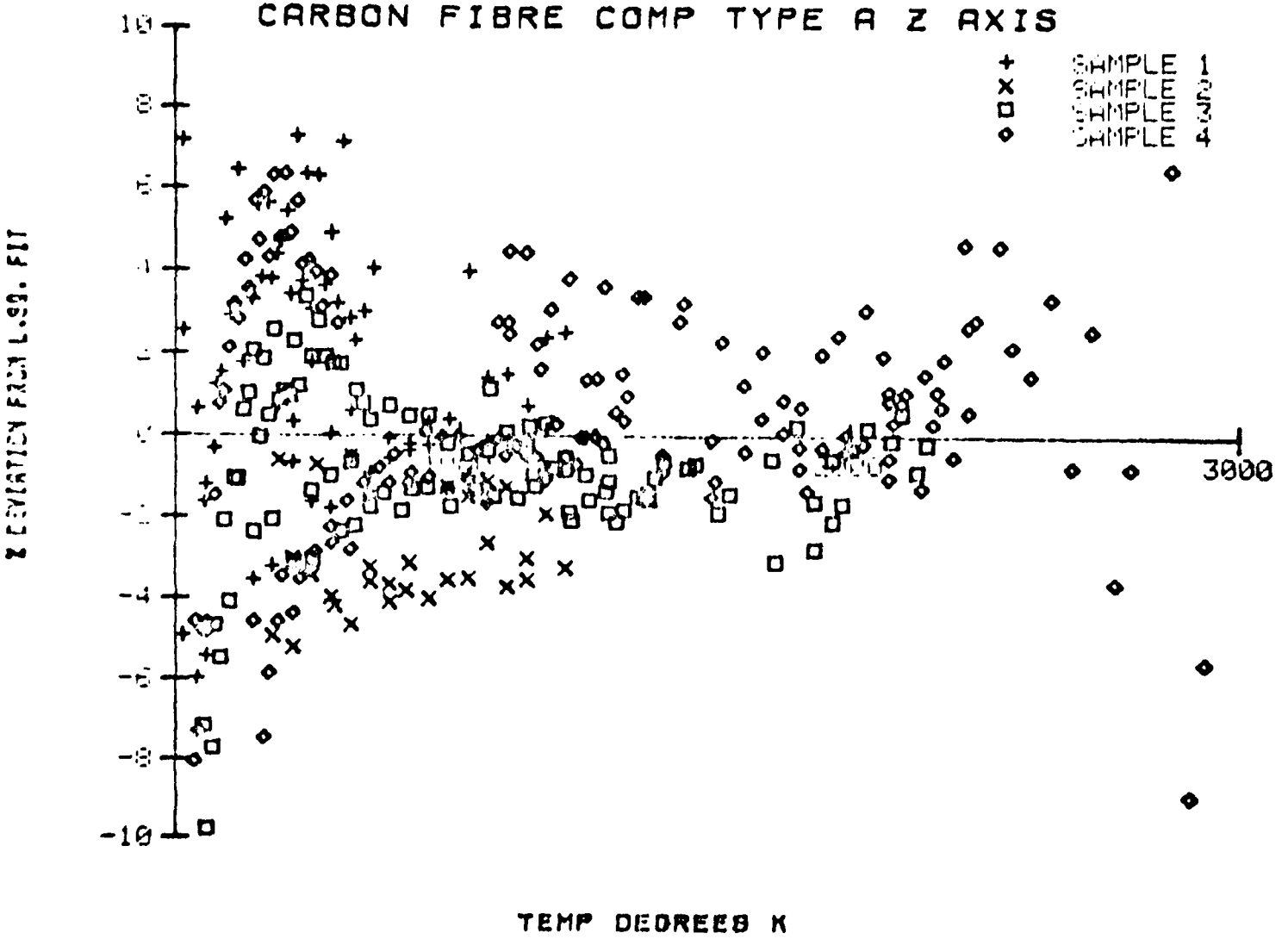
CARBON FIBRE COMP TYPE A Z AXIS
SAMPLE 1
10
-10
3000
% DEVIATION FROM L.SQ. FIT
TEMP DEGREES K

Figure 9

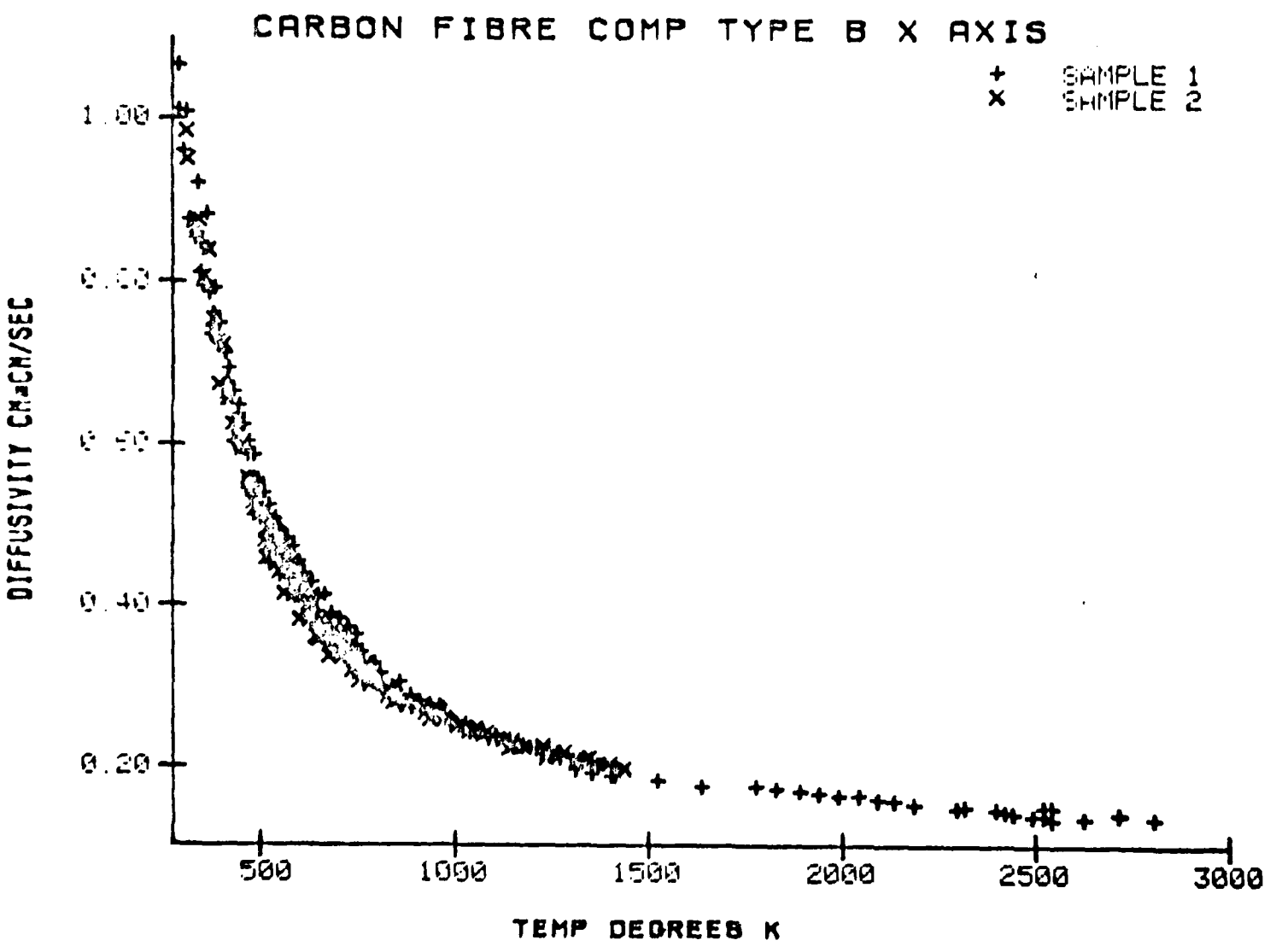
CARBON FIBRE COMP TYPE B X AXIS
+ SAMPLE 1
× SAMPLE 2
1.00
0.60
0.40
0.20
DIFFUSIVITY CM*CM/SEC
500
1000
1500
2000
2500
3000
TEMP DEGREES K

Figure 10

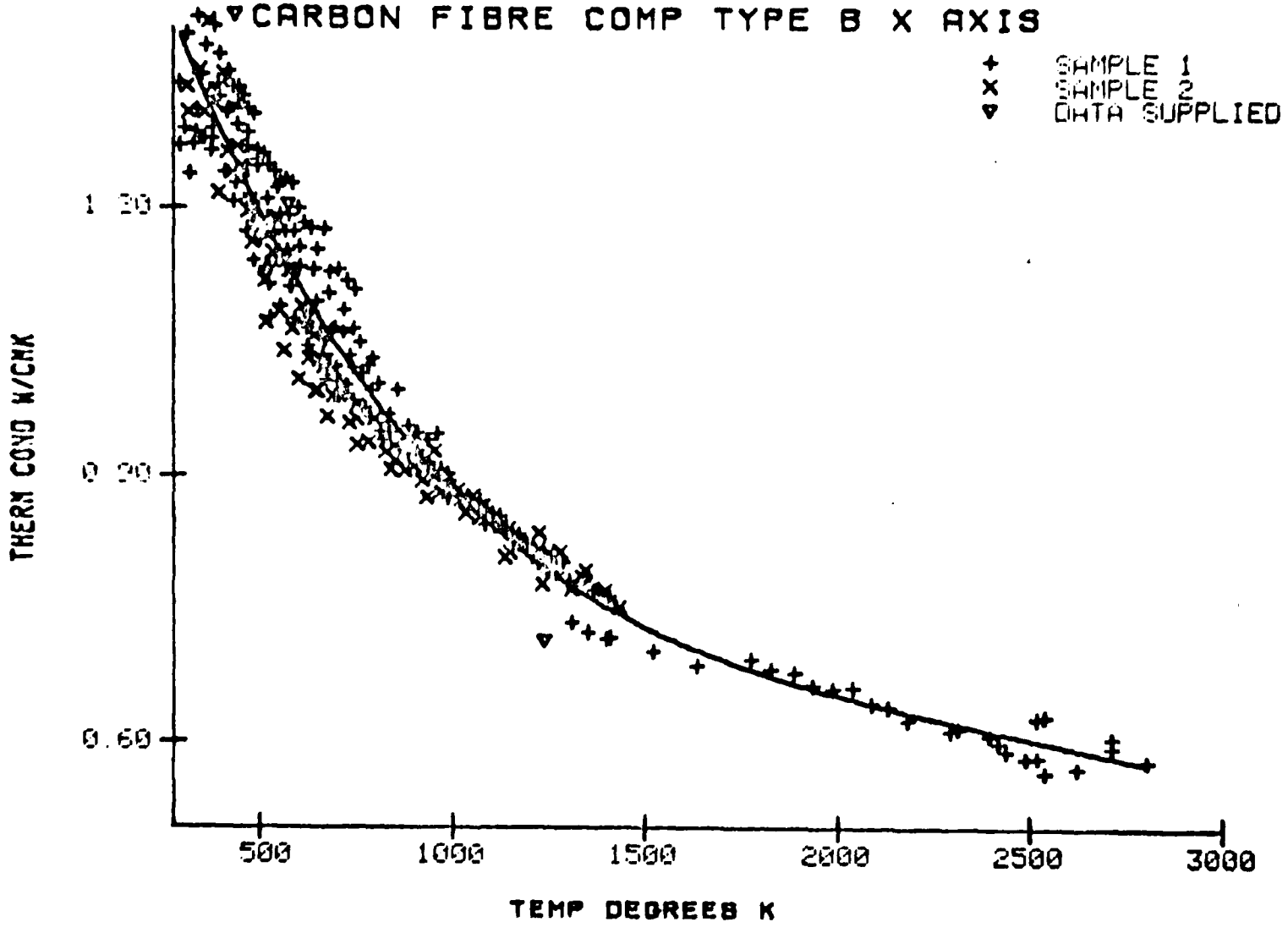
CARBON FIBRE COMP TYPE B X AXIS
SAMPLE 1
SAMPLE 2
DATA SUPPLIED
THERM COND W/CMK
1.20
0.90
0.60
500
1000
1500
2000
2500
3000
TEMP DEGREES K

Figure 11

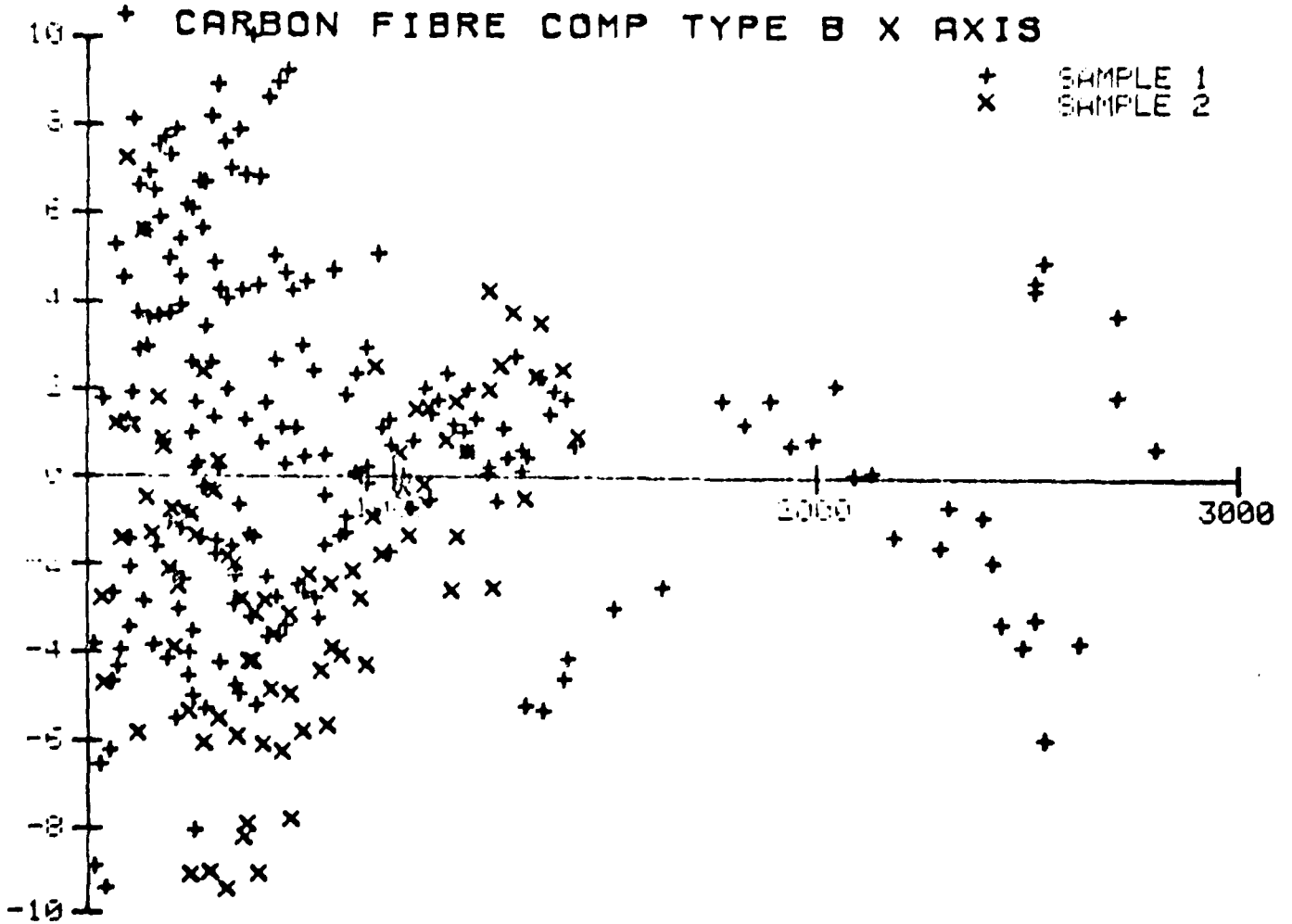
CARBON FIBRE COMP TYPE B X AXIS
SAMPLE 1
SAMPLE 2
10
-10
3000
% DEVIATION FROM L.SQ. FIT
TEMP DEGREES K

Figure 12

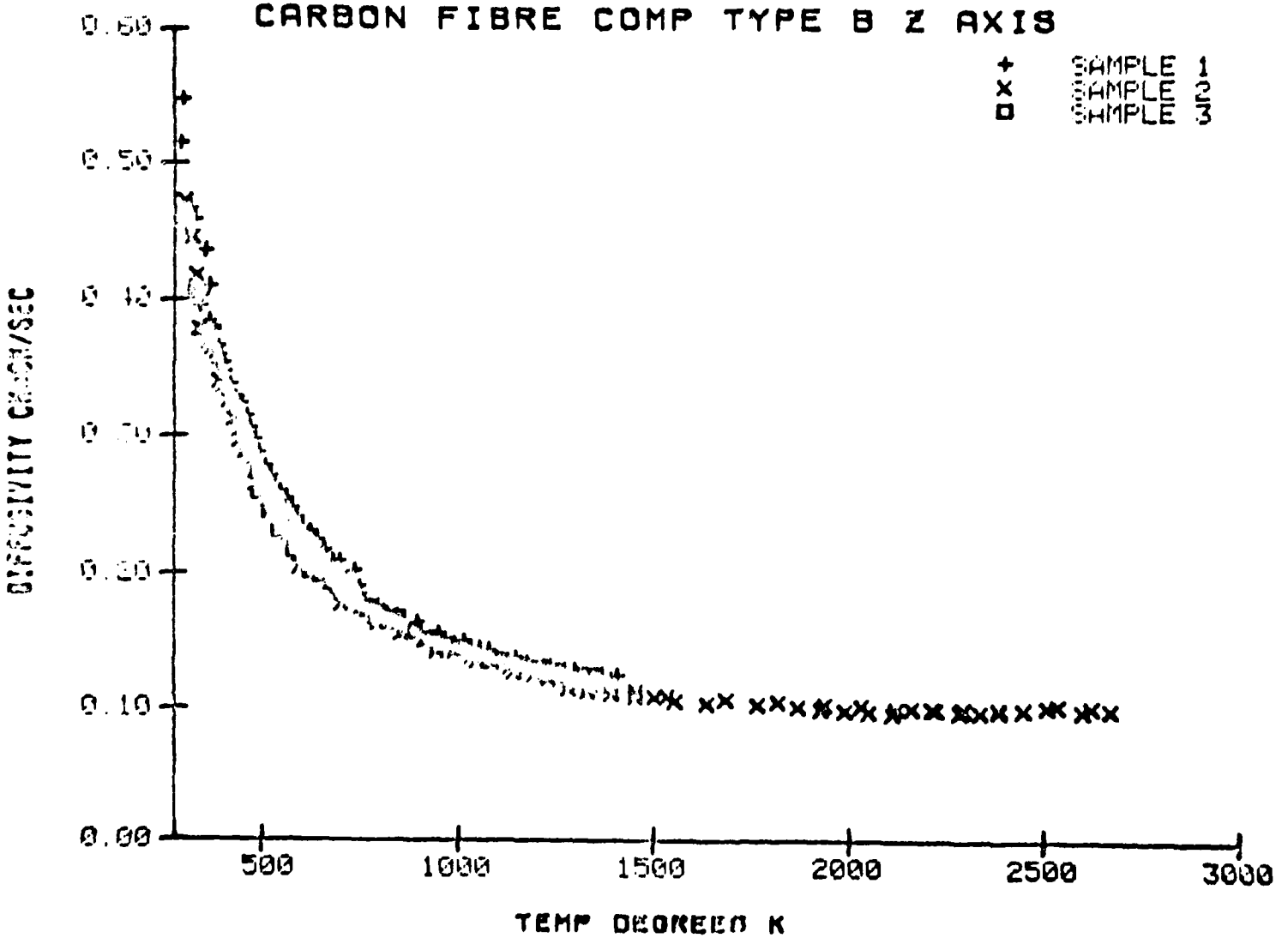
CARBON FIBRE COMP TYPE B Z AXIS
SAMPLE 1
SAMPLE 2
SAMPLE 3
0.50
0.10
0.00
500
1000
1500
2000
2500
3000
TEMP DEGREES K

Figure 13

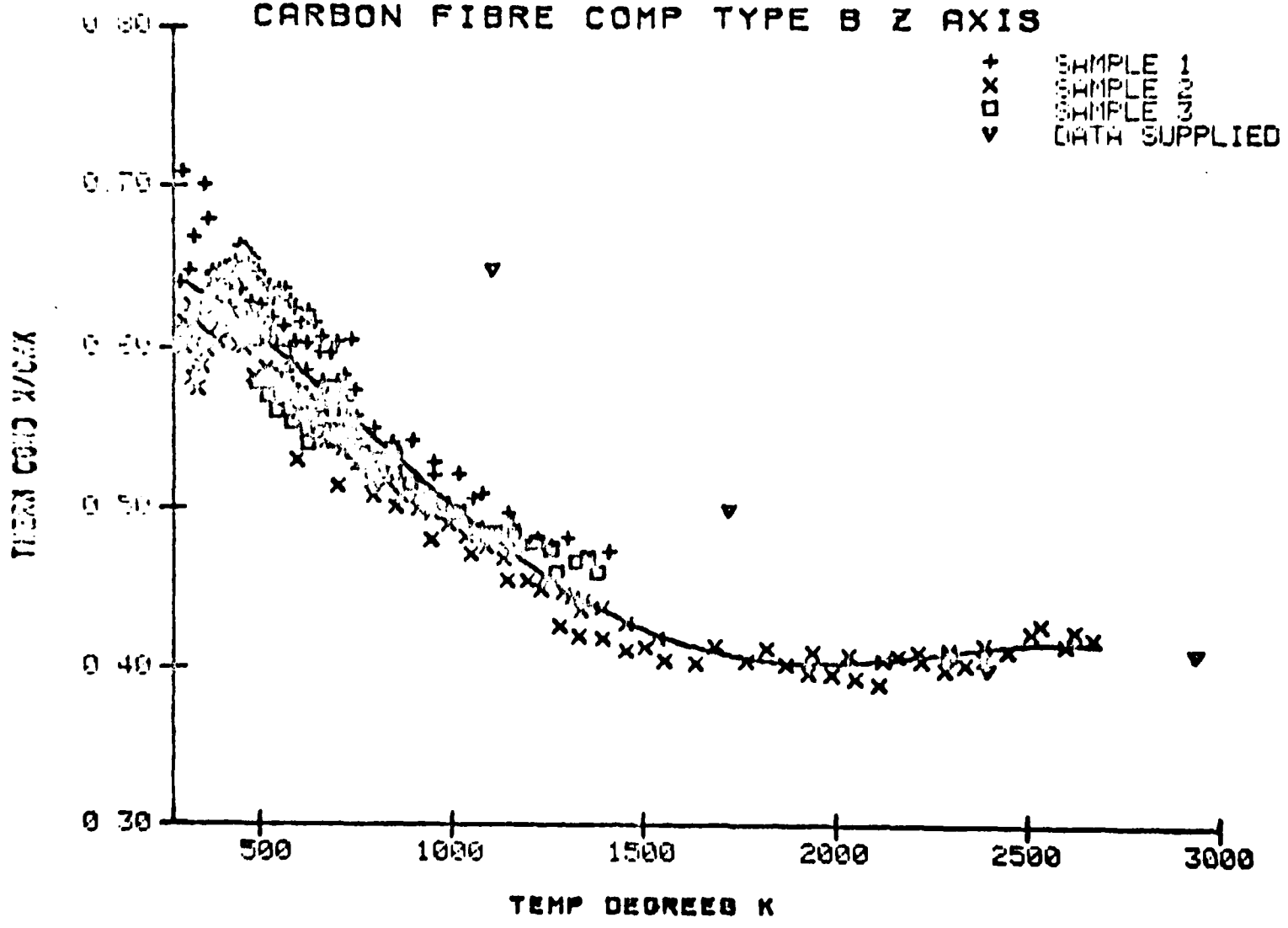
CARBON FIBRE COMP TYPE B Z AXIS
SAMPLE 1
SAMPLE 2
SAMPLE 3
DATA SUPPLIED
0 80
0 70
0 50
0 40
0 30
500
1000
1500
2000
2500
3000
TEMP DEGREES K

Figure 14

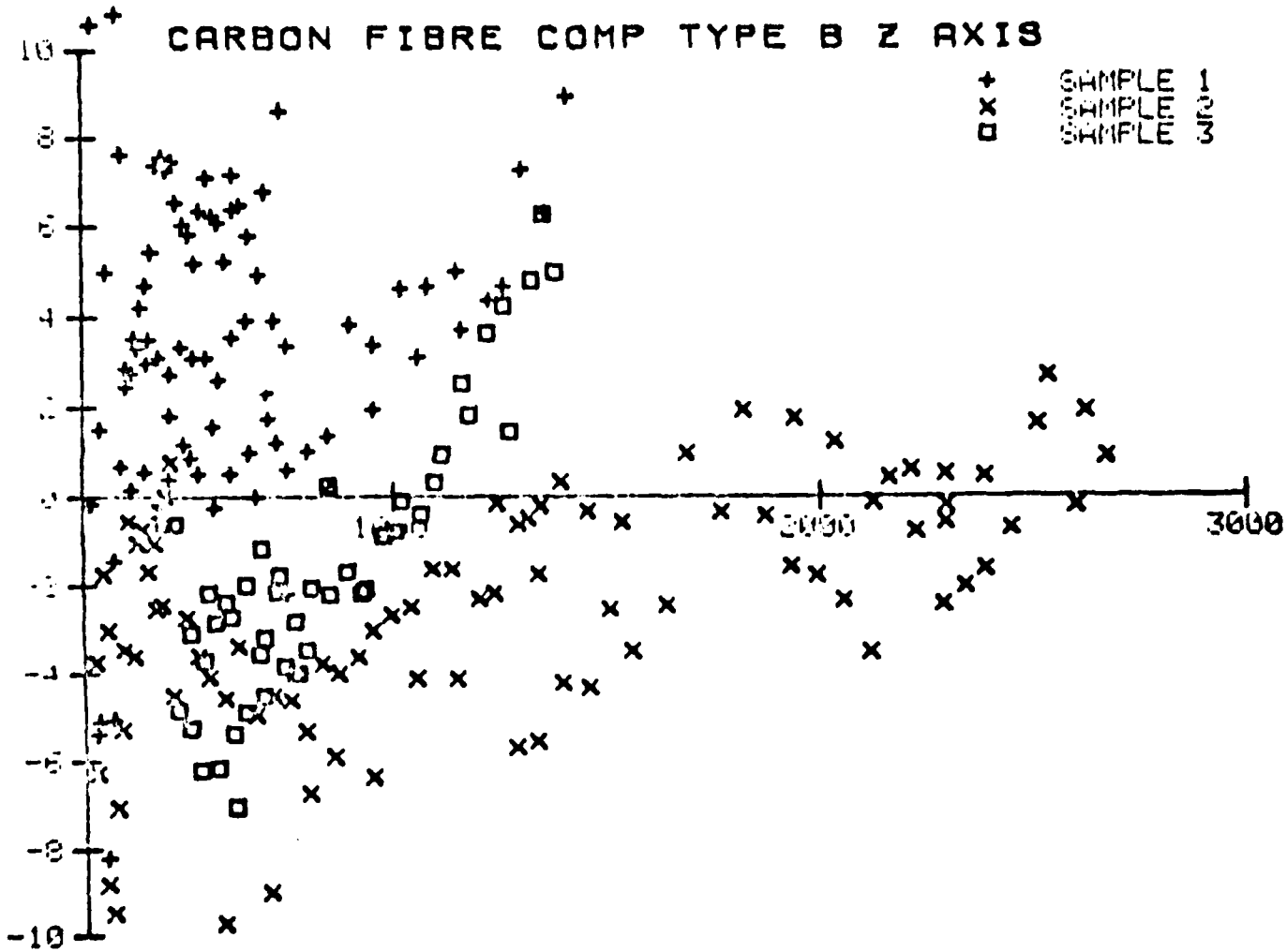
CARBON FIBRE COMP TYPE B Z AXIS
SAMPLE 1
SAMPLE 2
SAMPLE 3
10
8
6
4
2
0
-2
-4
-6
-8
-10
1000
2000
3000
% DEVIATION FROM L.S.Q. FIT
TEMP DEGREES K

Figure 15

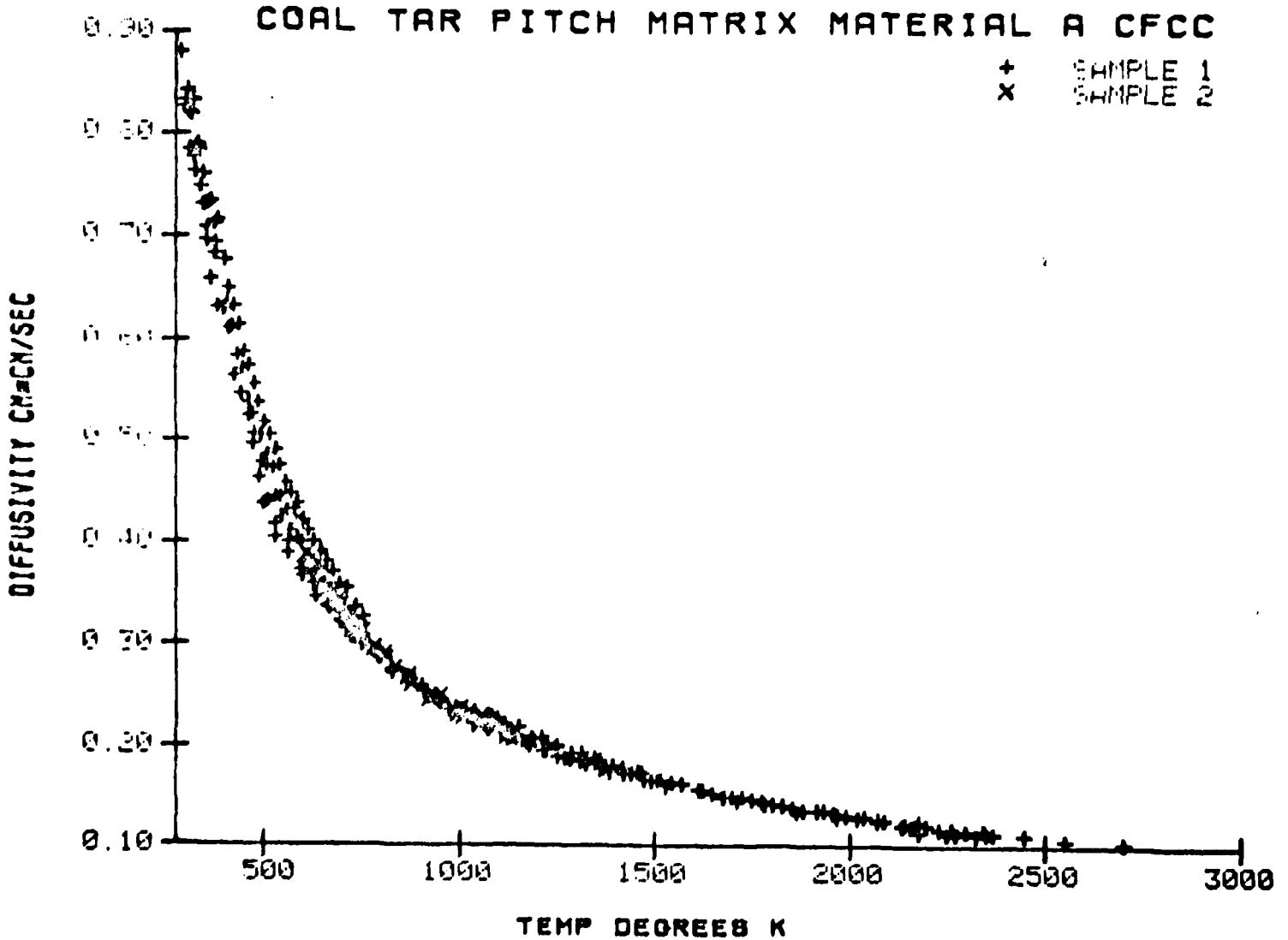
COAL TAR PITCH MATRIX MATERIAL A CFCC
+ SAMPLE 1
X SAMPLE 2
DIFFUSIVITY CM=CM/SEC
0.10
500
1000
1500
2000
2500
3000
TEMP DEGREES K

Figure 16

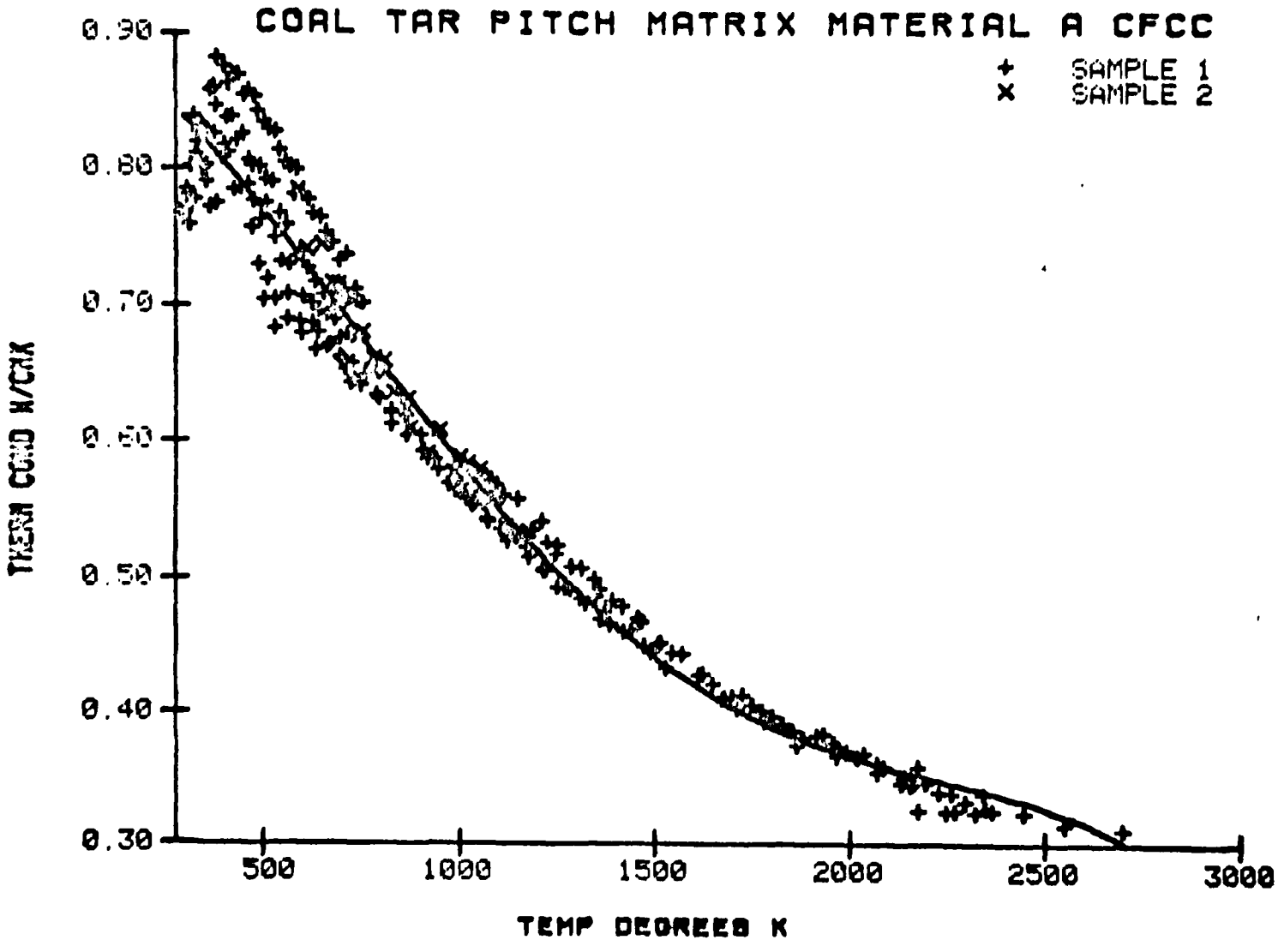
COAL TAR PITCH MATRIX MATERIAL A CFCC
+ SAMPLE 1
× SAMPLE 2
0.90
0.80
0.70
0.60
0.50
0.40
0.30
THERM COND W/CMK
500
1000
1500
2000
2500
3000
TEMP DEGREES K

Figure 17

matrix material within the composite. Evidence suggests in general that the density of carbon composite phases in situ is higher than when processed individually[10]. However, the matrix 'crossover' pockets (see Figure 1) are known to have porosity values of between 10-50%[6].

The matrix conductivity is very similar to that of POCO graphite type AXM-5Q1, a well documented reference material[9]. With an average density of 1.75 grms/cm^3, the POCO porosity is considerably lower, however. Whilst radiative and gaseous conduction modes may become important in high porosity, low conductivity materials[1] no enhancement of the matrix thermal properties was observed in a helium atmosphere both at low and high temperatures. Similarly, such expressions as are available to quantify radiative conduction in porous materials suggest that this too would be insignificant in the present case.

(D) 1-D Composite

(i) Axis Parallel with Fibres

Diffusivity and conductivity results from two parallel(//) axis samples are shown in Figures 18 and 19. No comparative data is available.

The 1-D composite was unique in that its properties change significantly after heating to temperatures > 2300K. Spot measurements, at temperatures of 600-700K, were made after the principal measurements had been completed. These revealed that the diffusivity of both samples was reduced to 50% or less of its original value. In addition there was a permanent change in sample length and diameter of ~1-1.5% respectively.

Since there are no orthogonal yarn influences, it is expected that the 1-D composite thermal expansion be higher than that of the 3-D materials[6]. However, no permanent offsets have been reported before. Significantly, it is now known that the processing of the 1-D material differs from that of the other composites[6] reported here.

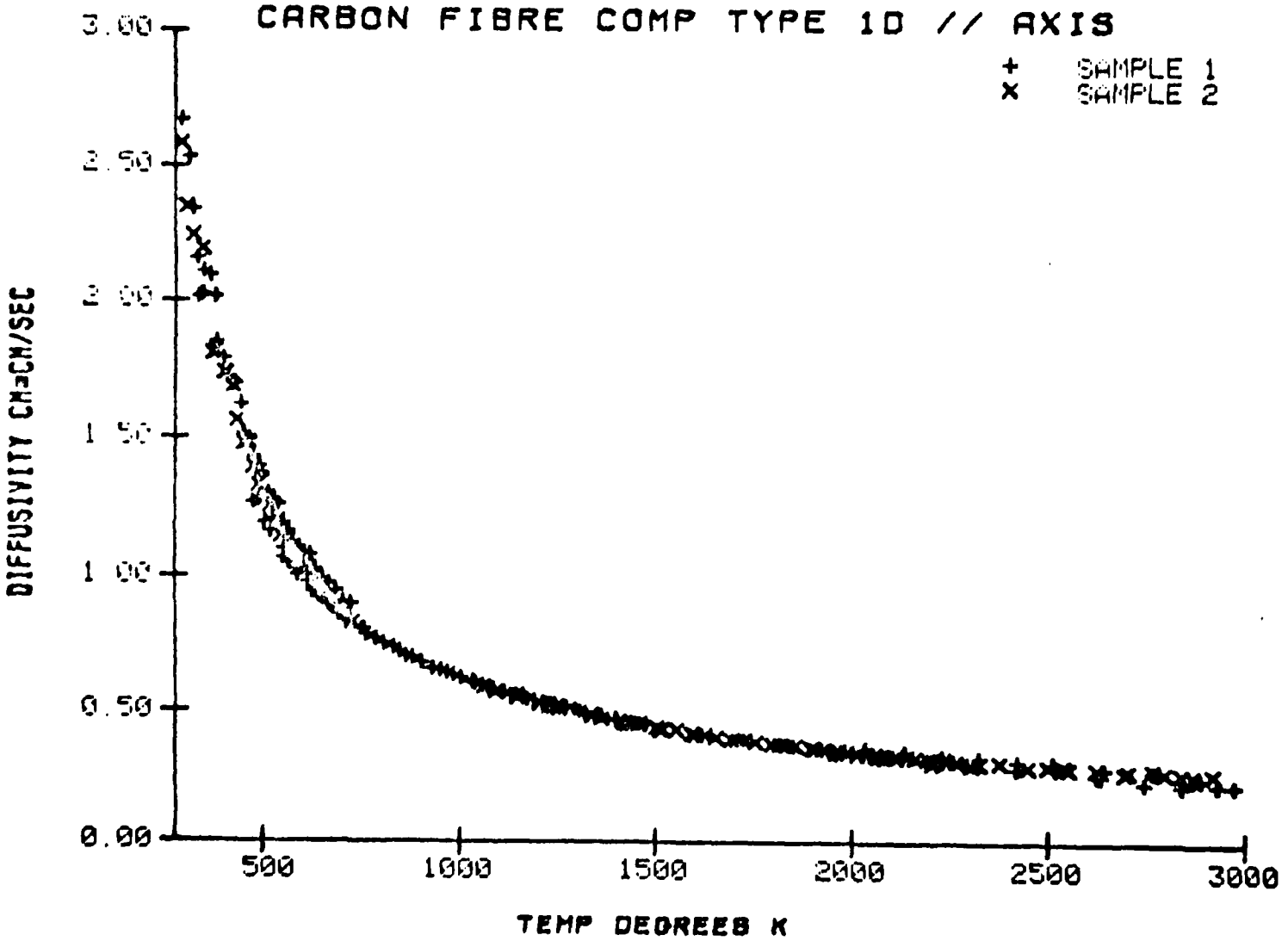
CARBON FIBRE COMP TYPE 1D // AXIS
+ SAMPLE 1
× SAMPLE 2
3.00
2.50
2.00
1.50
1.00
0.50
0.00
DIFFUSIVITY CM²CM/SEC
500
1000
1500
2000
2500
3000
TEMP DEGREES K

Figure 18

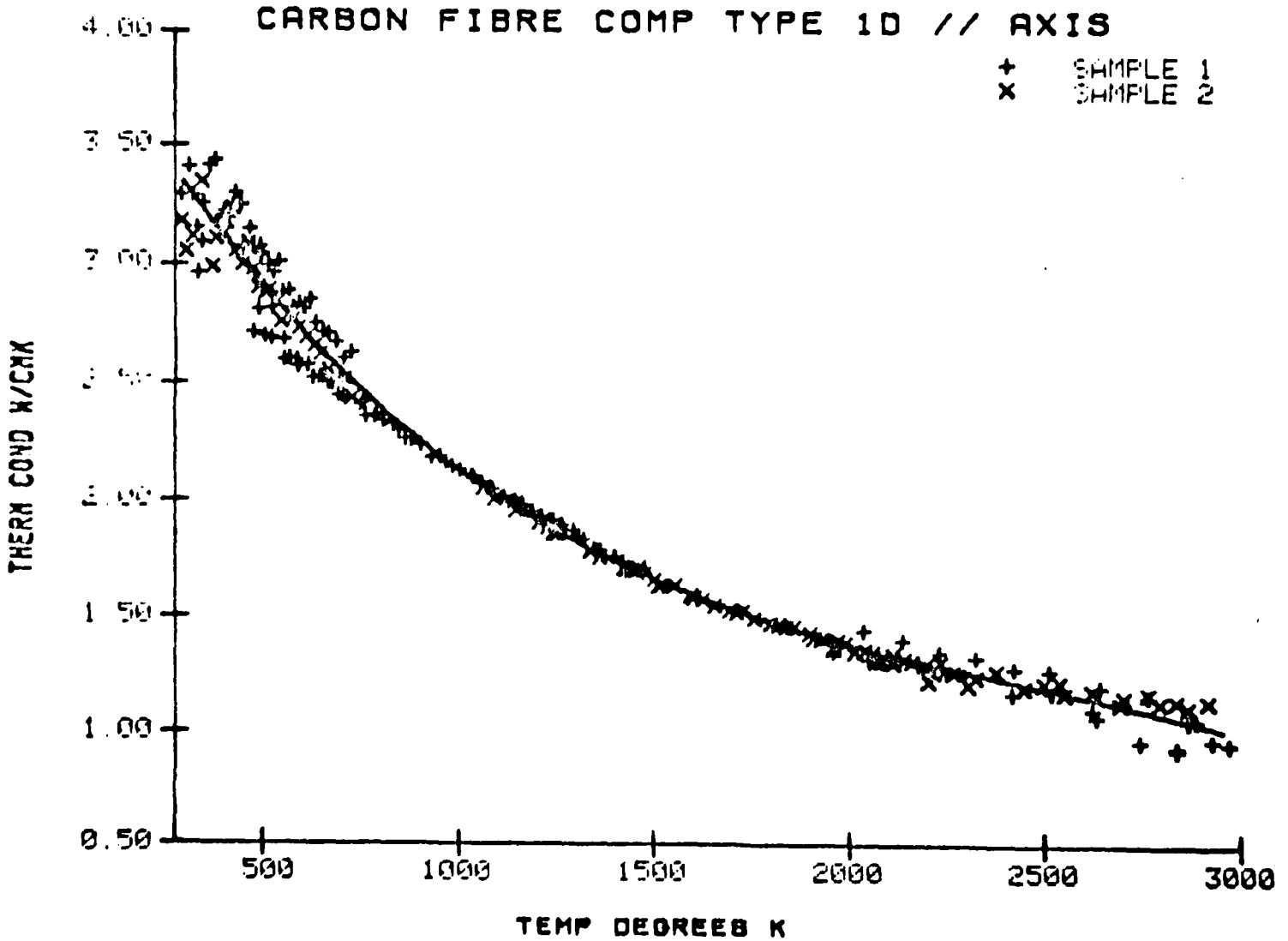
CARBON FIBRE COMP TYPE 1D // AXIS
+ SAMPLE 1
× SAMPLE 2
THERM COND W/CMK
4.00
3.50
3.00
2.50
2.00
1.50
1.00
0.50
500
1000
1500
2000
2500
3000
TEMP DEGREES K

Figure 19

Typically, the high temperature (2000-3000K) measurement runs lasted 2-3 hours. Oxygen contamination has been ruled out since other sample types were not effected.

Subsequent liquid densitometer measurements showed a density increase of about 1%. Compared with the nominal decrease in bulk density, this indicates a decrease in closed porosity and microstructural changes.

The high conductivity of the 1-D parallel axis is another surprising feature. The room temperature value of approximately 3.0 W/cmK must be compared with available data on Fibre 'F' conductivity which indicates a value of ≈ 0.6 W/cmK along the fibre axis[2,6,11]. This large difference in the properties of the 1-D composite and fibres has important implications and will be discussed more fully when composite modelling techniques are examined.

There are doubts as to the efficacy of diffusivity measurements on highly orientated composites where the integrity of conduction paths is preserved. A good example of this is the parallel axis of the 1-D composite. Arguably, an effective composite diffusivity does not exist for such materials in which event the rear face temperature analysis (see Equation 2) will give meaningless results, except in two extreme cases. These are:

1) $\alpha_1 \approx \alpha_2$

2) $\alpha_1 >> \alpha_2$

where α_1 and α_2 are the diffusivities of the phases.

Case 2) has been used by Taylor[2] to measure the diffusivity of carbon fibres.

The rear face temperature analysis enables the calculation of diffusivity with any value of x ($0<x<1$) in t_x provided the appropriate value of w/π^2 is used in Equation 2. Calculation of diffusivity for different values of x gives a check on how closely the observed transient conforms to its theoretical form and thus may provide information as to the nature of the sample.

The rear face temperature transients of several 1-D composite samples were recorded over a temperature range where heat losses would not distort the transient. The difference in diffusivity values calculated from t_x values in the range $0.2 < t_x < 0.8$ was less than ±4%. It may be concluded therefore that the parallel axis does have a meaningful effective diffusivity.

(ii) Axis Transverse to Fibres

Diffusivity and conductivity results for the transverse fibre (TF) axis from three samples are shown in Figures 20 and 21.

Figure 22 shows % deviation from least square fit (see Table 5) by sample number. There is no apparent correlation with sample density (see Table 4).

The TF axis samples also showed irreversible dimension changes after heating to 2400K. Changes in sample length were in the range of 2.6-4.9%. Fibre thermal expansion is known to be higher in the transverse direction[6,12].

7. MICROSTRUCTURAL INVESTIGATION

Figures 23 and 24 show Scanning Electron Microscope (SEM) views across the fibre axis of two 1-D composite samples. The latter is sample 2 after measurements up to 2900K, and the former has undergone no heating. There were no obvious signs of microstructural changes which could explain the large transverse offset. For example, fibre/matrix interfaces appeared very similar with no evidence of increased separation, as higher magnification shows (see Figures 25 and 26).

Figure 27 shows a general view across the X axis of an unheated specimen of CFCC 'A'. The fibre yarns running from bottom left to top right are the Y axis reinforcement and the remaining are Z axis yarns. Pores of up to 100 μm size were clearly visible within the matrix 'cross-over' pockets.

Broken yarn/yarn interfaces were a common feature of the 3-D composites as Figure 28 illustrates whereas yarn/matrix interfaces were

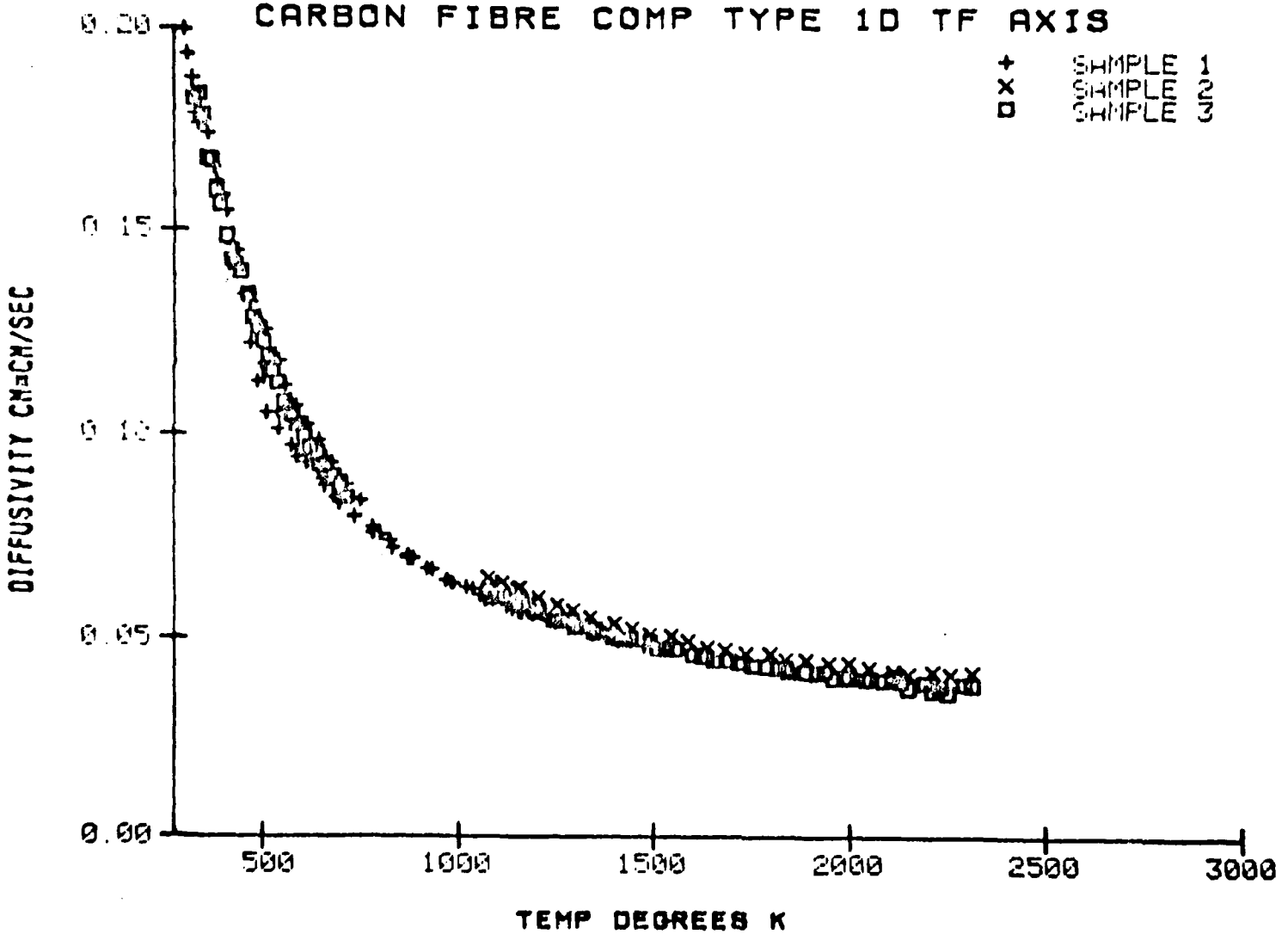
CARBON FIBRE COMP TYPE 1D TF AXIS
+ SAMPLE 1
X SAMPLE 2
□ SAMPLE 3
0.20
0.15
0.10
0.05
0.00
DIFFUSIVITY CM=CM/SEC
500
1000
1500
2000
2500
3000
TEMP DEGREES K

Figure 20

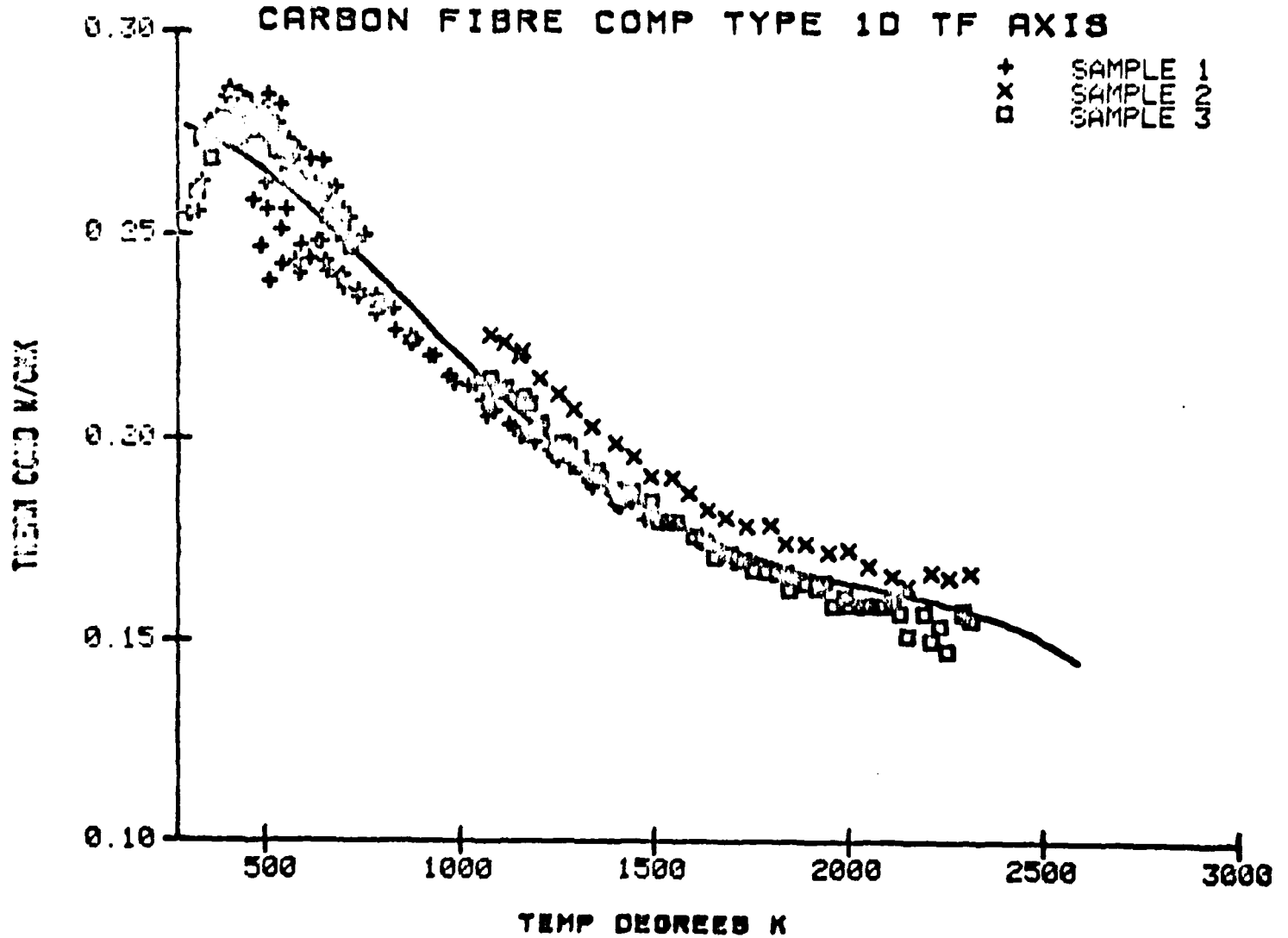
CARBON FIBRE COMP TYPE 1D TF AXIS
SAMPLE 1
SAMPLE 2
SAMPLE 3
0.30
0.25
0.20
0.15
0.10
500
1000
1500
2000
2500
3000
TEMP DEGREES K

Figure 21

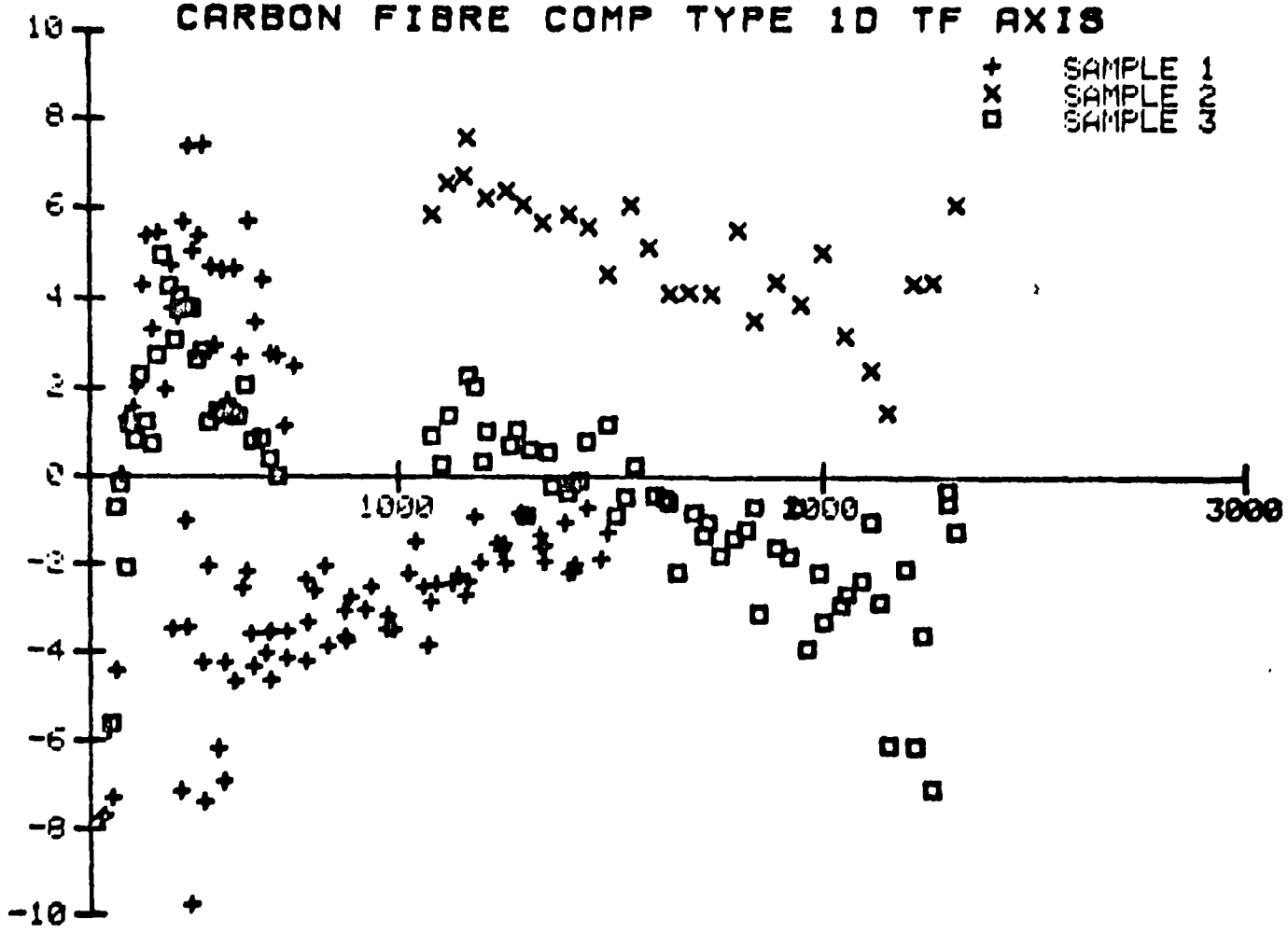
CARBON FIBRE COMP TYPE 1D TF AXIS
SAMPLE 1
SAMPLE 2
SAMPLE 3
10
8
6
4
2
0
-2
-4
-6
-8
-10
1000
2000
3000
% DEVIATION FROM L.S.I. FIT
TEMP DEGREES K

Figure 22

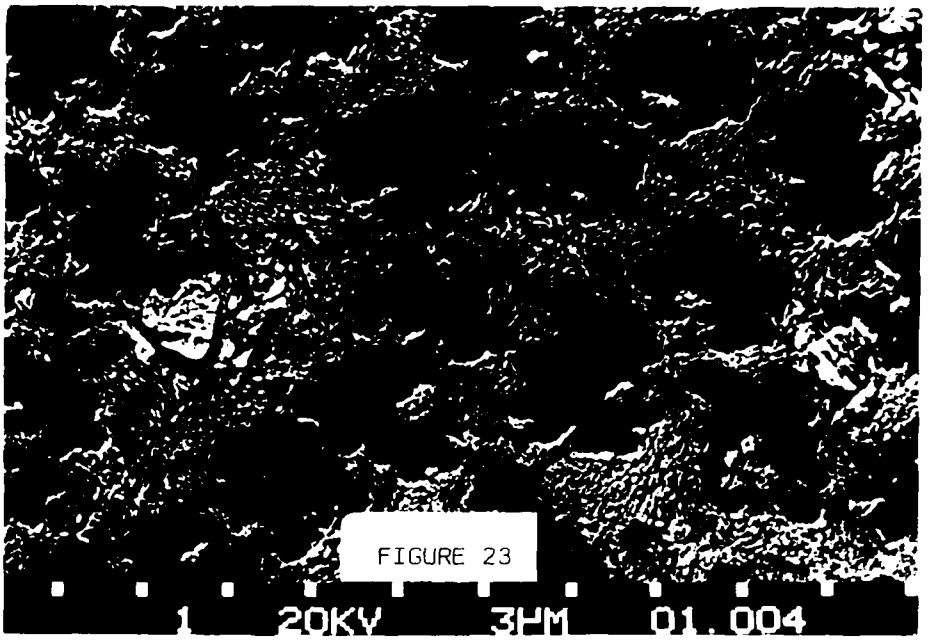

FIGURE 23

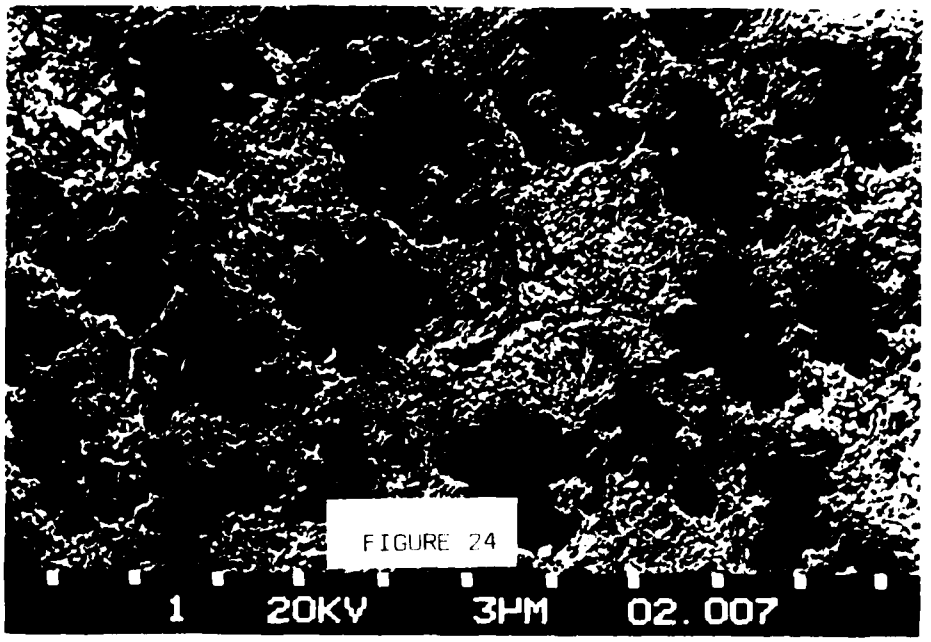

FIGURE 24

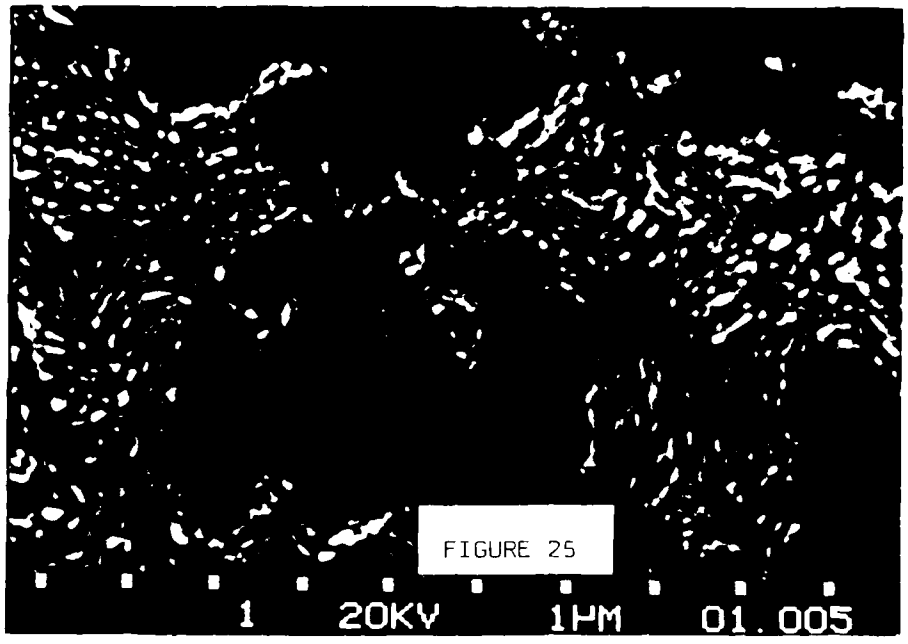
FIGURE 25
1 20KV 1HM 01.005

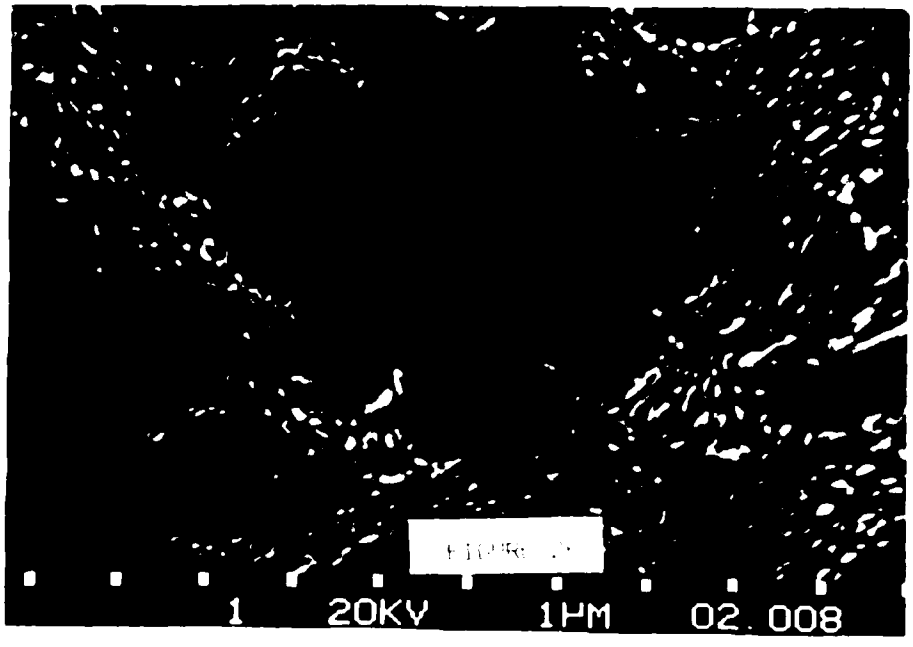
1 20KV 1HM 02.008

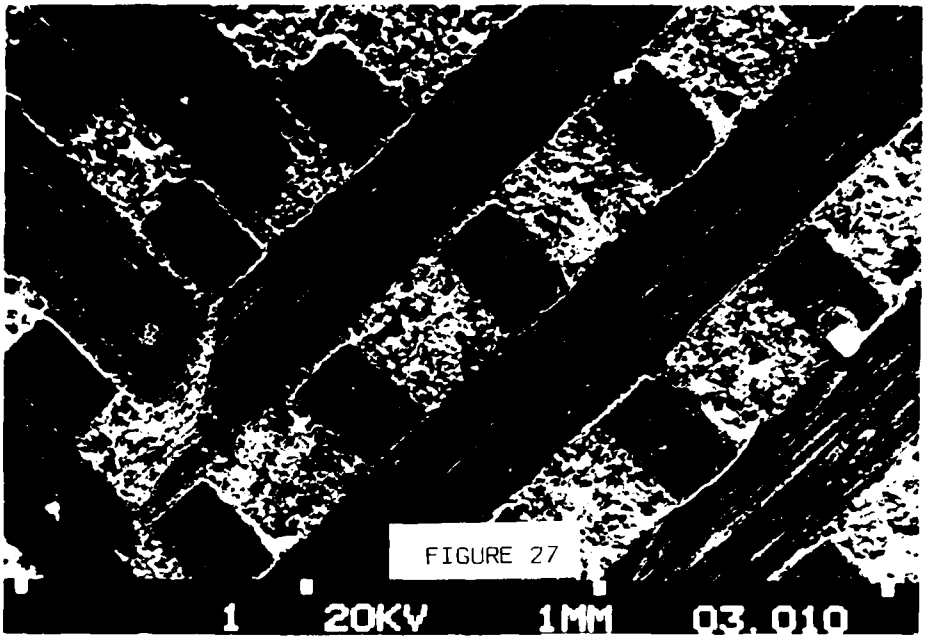

FIGURE 27

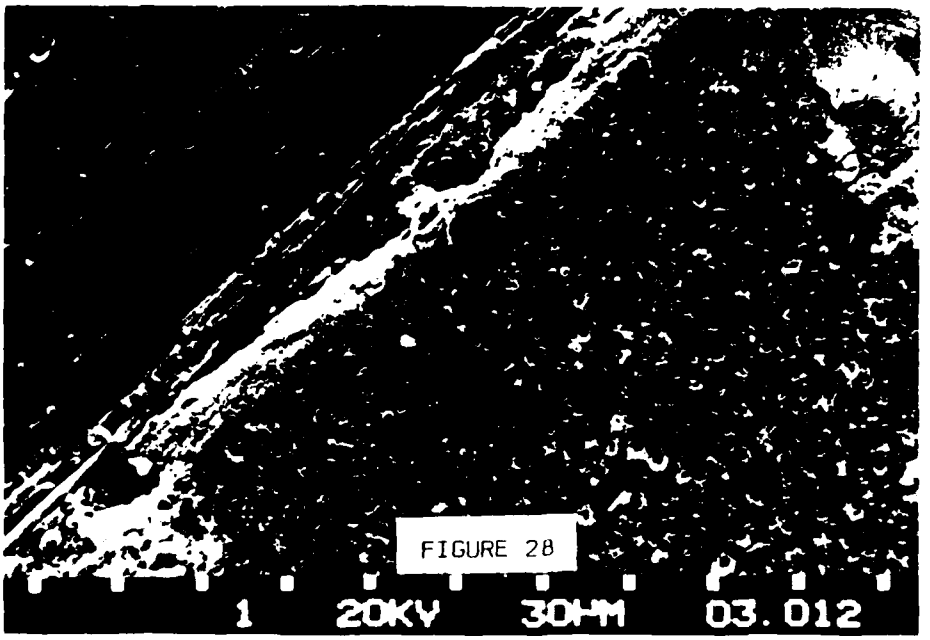

FIGURE 28

generally intact. The X axis reinforcement is composed of two yarns, but there was little evidence of yarn splitting in the unheated composite.

Figure 29 shows greater separation between fibres and matrix than was visible in the 1-D composite. In some regions, the volume between adjacent fibres was completely filled by material of an apparently different form to the rest of the matrix (see Figure 30). This most probably is CVD material[6].

A general view across the 'Z' axis of a CFCC 'A' specimen that had been measured up to 2900K is shown in Figure 31. Splitting within the 'Z' axis yarns could be seen and the pattern of broken yarn/yarn interfaces repeated but clearly more marked than in the unheated specimen (Figure 32). However, spot diffusivity measurements on cooling revealed no measureable impact on thermal properties.

No evidence could be seen of changes in the fibre/matrix interface (Figure 33).

A general view across the X axis of CFCC 'B' is shown in Figure 34, illustrating the different fabrication method of this composite. The X reinforcements were not easy to distinguish individually because of the apparent absence of matrix 'crossover' pockets. The area between the Z yarns appeared remarkably homogeneous, a feature further illustrated in Figure 35. Presumably, this is a result of using a weave instead of orthogonal fibres held in place before CVD by a jig[6]. The X and Y reinforcements are therefore able to expand into the crossover pockets otherwise filled by the matrix. The vertical cracks, both major and minor, were regularly spaced and probably mark the boundaries between adjacent X-Y reinforcement planes which are nominally 0.254 mm (254 μm) thick.

Broken Z yarn/X-Y place interfaces were quite prominent and the fibre/matrix microstructure was very similar to that of CFCC 'A'.

Figure 36 shows a general view across the Z axis, illustrating the fine weave pierced fabric (FWPF) construction. Broken yarn/yarn interfaces are

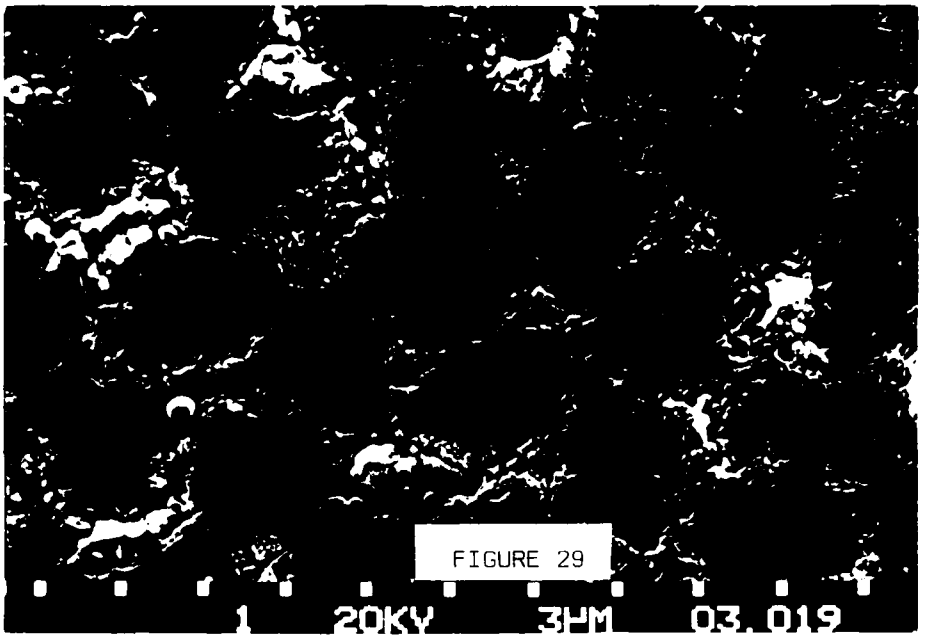

FIGURE 29

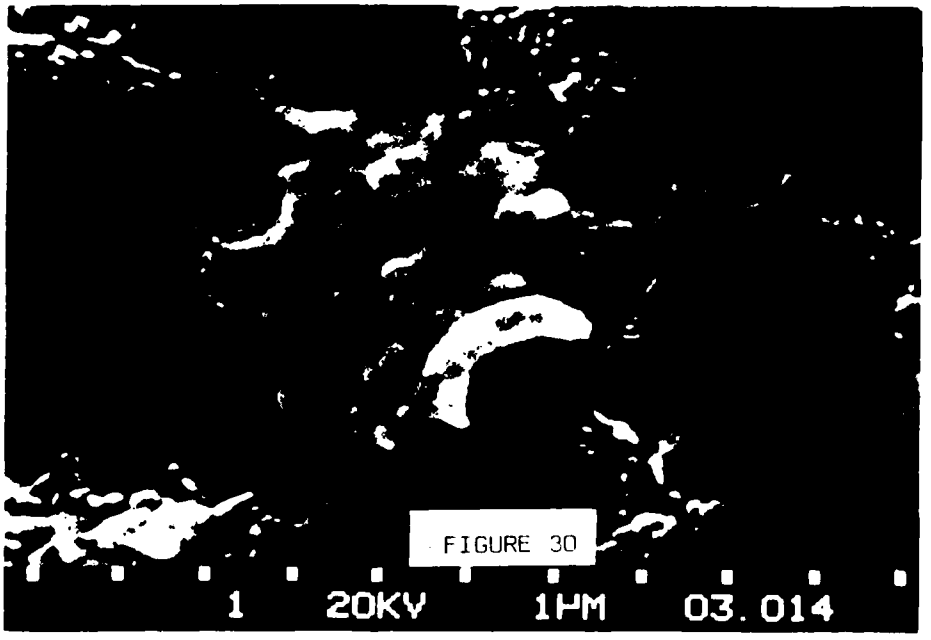

FIGURE 30

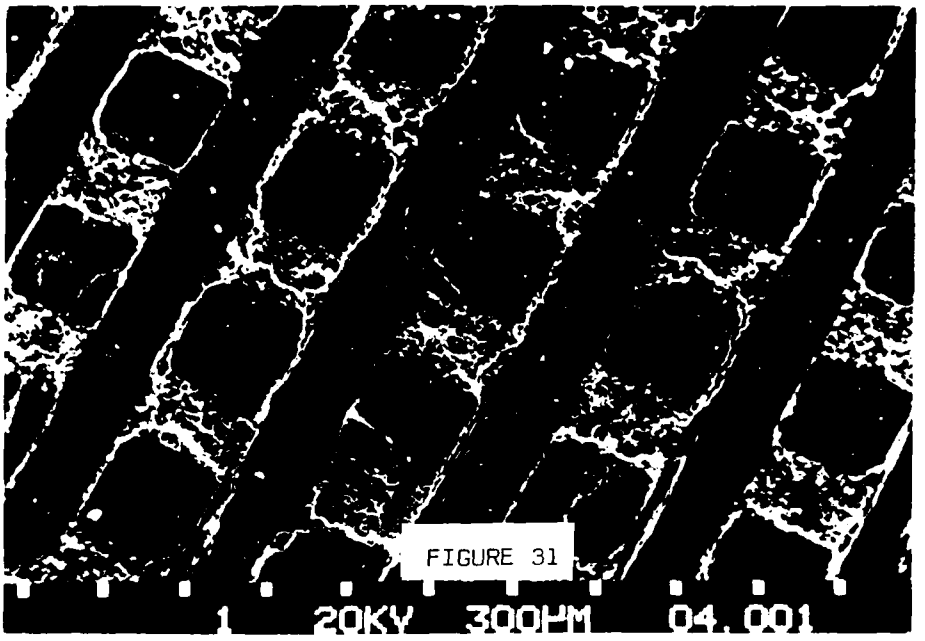

FIGURE 31

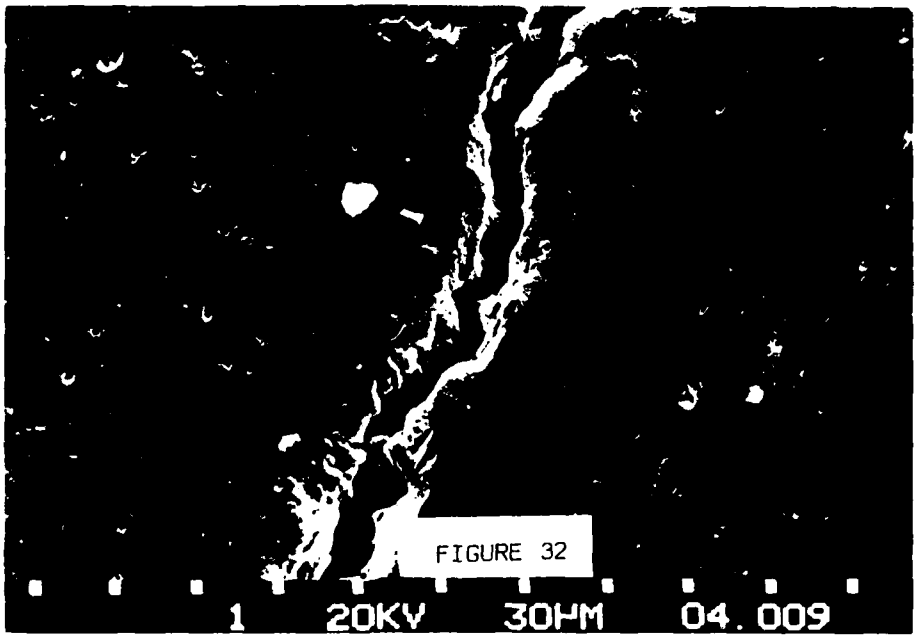

FIGURE 32

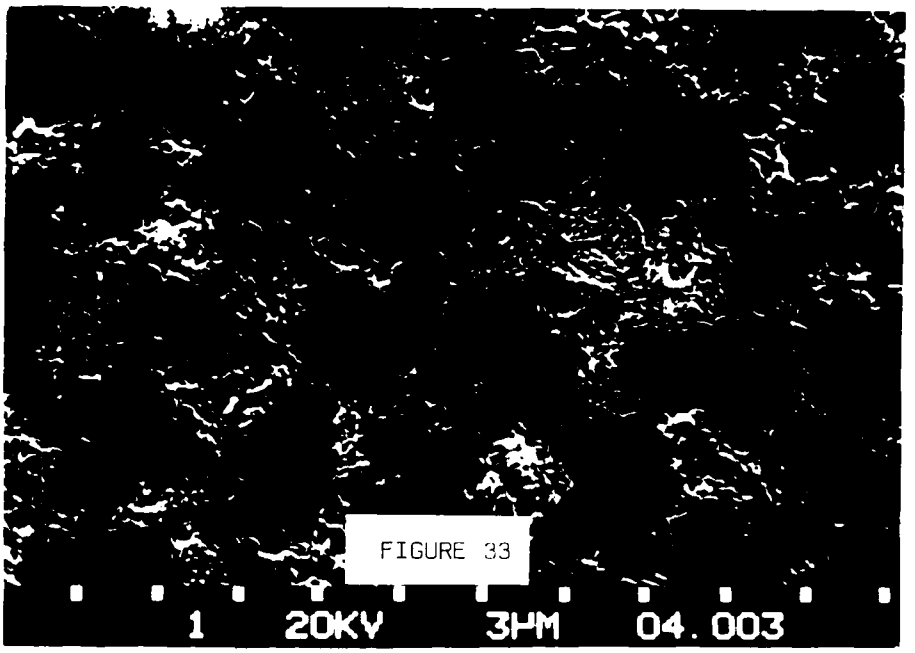

FIGURE 33

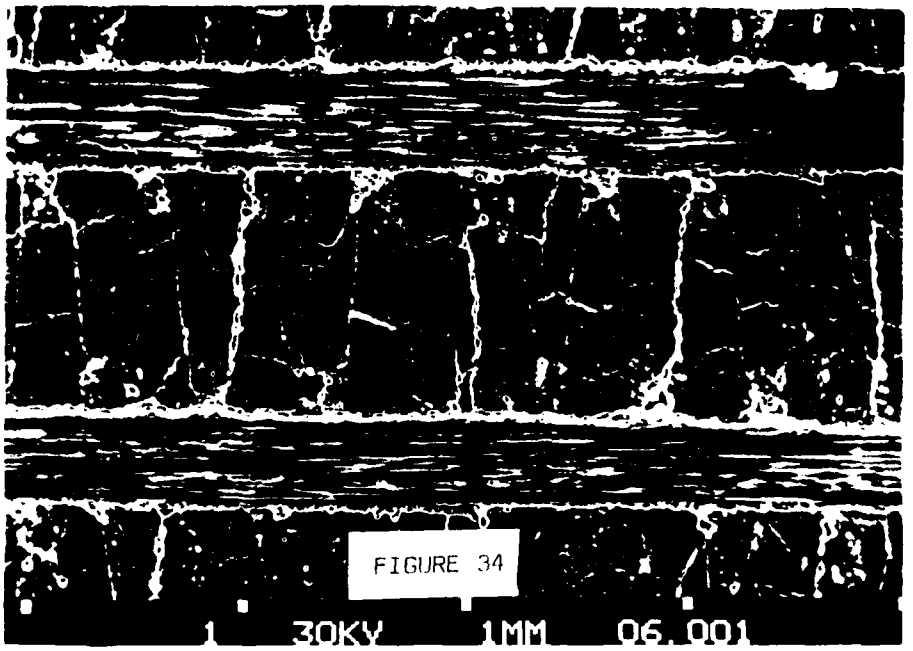

FIGURE 34

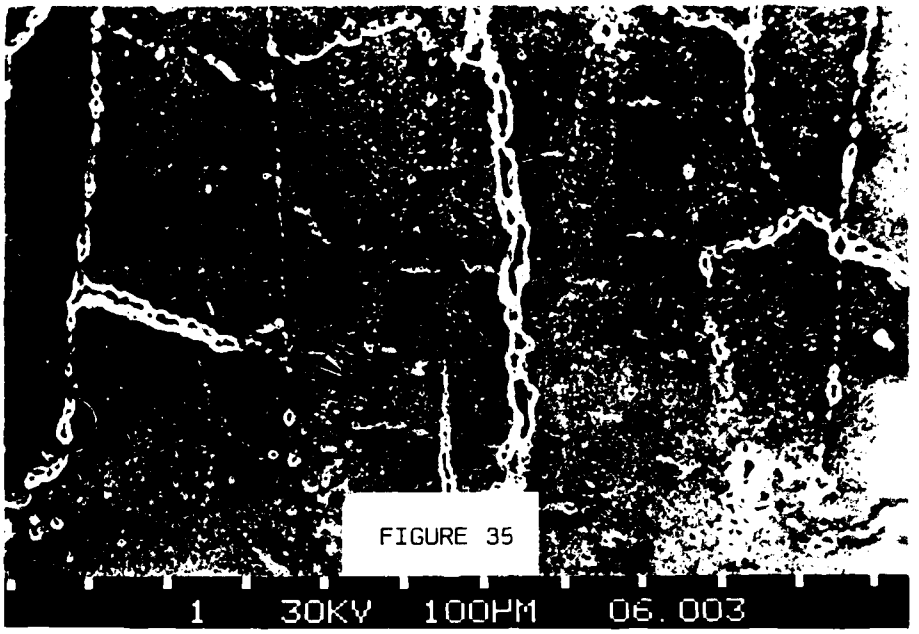

FIGURE 35

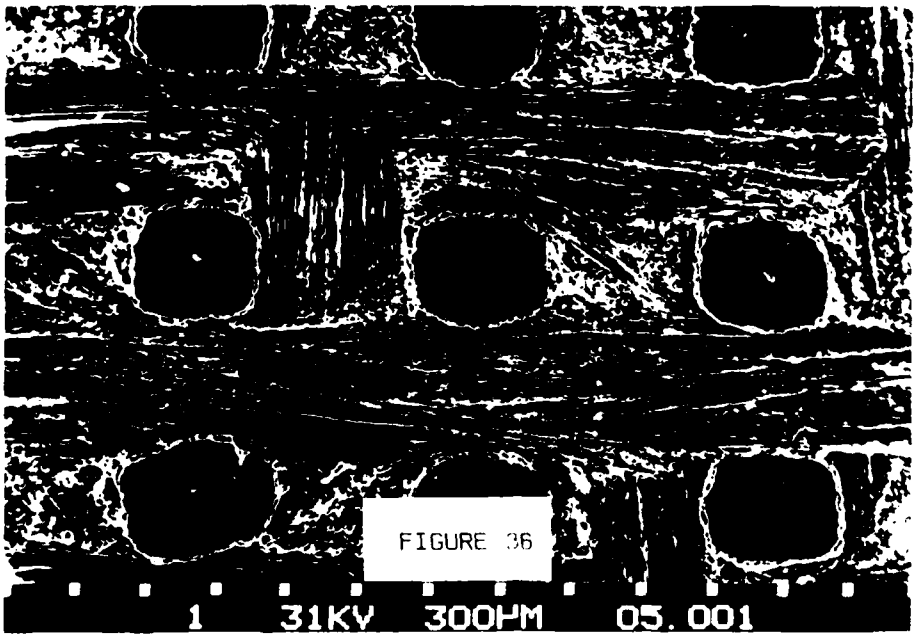

FIGURE 36

again visible.

Finally, Figure 37 shows a section through the bulk matrix material revealing a range of pore sizes up to 300 μm.

8. MODELLING OF CFCC THERMAL CONDUCTIVITY

(A) 1-D Composite

The thermal conductivity in the direction of reinforcement of a highly oriented 1-D composite may be simply analysed in terms of the volume weighted conductivities of the constituents[11]. Thus, using an Ohm's law approach:

$$\lambda_c = v_f \lambda_f + (1-v_f)\lambda_m \qquad (4)$$

where λ_c is the conductivity of the composite

λ_f is " " " " fibres

λ_m is " " " " matrix

v_f is the fibre volume fraction.

It is clear from the conductivity of the bulk matrix, reported here, and the known conductivity of fibre type 'F' (λ = 0.6 W/cmK at 300K) that the conductivities of the individual phases cannot in this case account for the conductivity of the composite. It is unlikely that the much higher composite conductivity (3.0 W/cmK at 300K) is due simply to the matrix restoring the integrity of fibre conduction paths by 'infill' of damaged and broken fibres.

The conductivity anisotropy ratio of the 1-D composite is approximately 12 at room temperature, decreasing to about 8 at 2300K. These are high values and if the bulk matrix properties are representative of the composite matrix, the implication must be that fibre anisotropy is also high.

Again using the so-called Ohm's law method, Springer and Tsai[13] have obtained a general equation for 1-D transverse conductivity, $\lambda_\perp$ (see

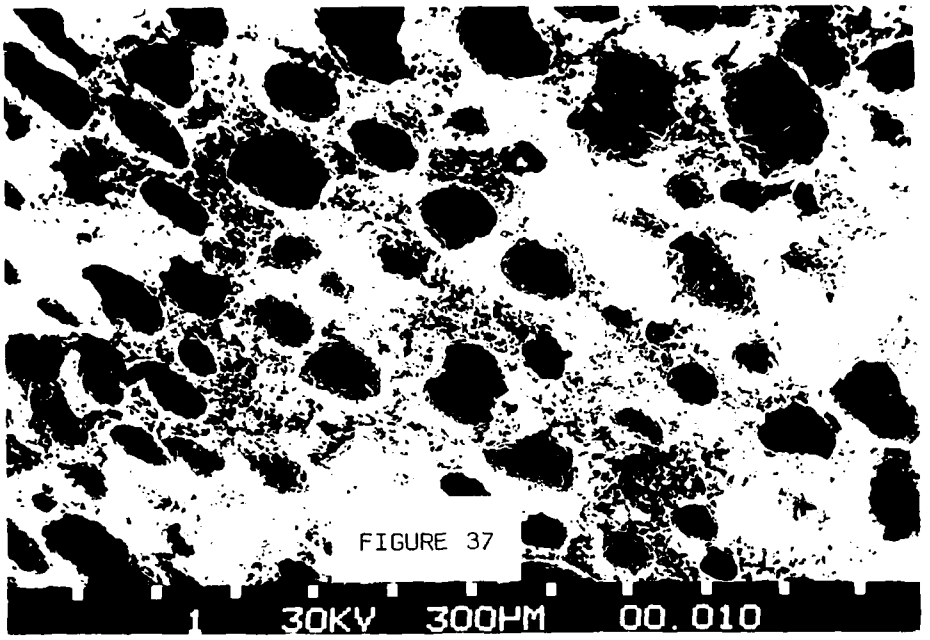

FIGURE 37

Figure 38).

$$\frac{\lambda_{\perp}}{\lambda_m} = \left(1 - \frac{d}{2b}\right) + \frac{a}{b}\int_o^d \frac{dy}{(2a-\beta) + (\beta\lambda_m/\lambda_{f\perp})} \qquad (5)$$

where $\beta = f(y)$, a function relating fibre width at any given y and $\lambda_{f\perp}$ is the fibre transverse conductivity. The solution of Equation 5 is shown graphically in Figure 38, for a fibre of circular cross-section and square packing, as a function of fibre volume fraction (FVF) and $\lambda_{f\perp}/\lambda_m$. Equation 5 assumes good contact between fibre and matrix but Figures 23-26 have shown this assumption to be quite appropriate for the 1-D composite.

The bulk matrix data gives a value for $\lambda_{\perp}/\lambda_m$ of 0.33 at room temperature and this leads to a value of about 0.1 for $\lambda_{f\perp}/\lambda_m$ at the appropriate FVF (0.53).

It has been reported[14] that matrix conductivity is usually below both axial and transverse fibre conductivity. This, if correct, is both surprising and at variance with the conclusions of the above analysis.

(B) 3-D Composites

The original approach of determining the thermal properties of the individual fibre and matrix phases and combing in the appropriate 3-D geometry is clearly invalidated by the 1-D composite experimental data. The reason is that it cannot take into account what is now known to be the influence of processing upon the properties of the constituent phases.

This may be qualitatively summarised as follows:

1) constituent densities tend to be significantly higher within the CFCC[6,10]. Increases of 20% and more have been reported in both matrix and fibres[10]. In the case of the fibres, some of this density increase is due to the filling of pores in the fibre bundles[15].

2) If used, the CVD process produces a sheath-like coating around the

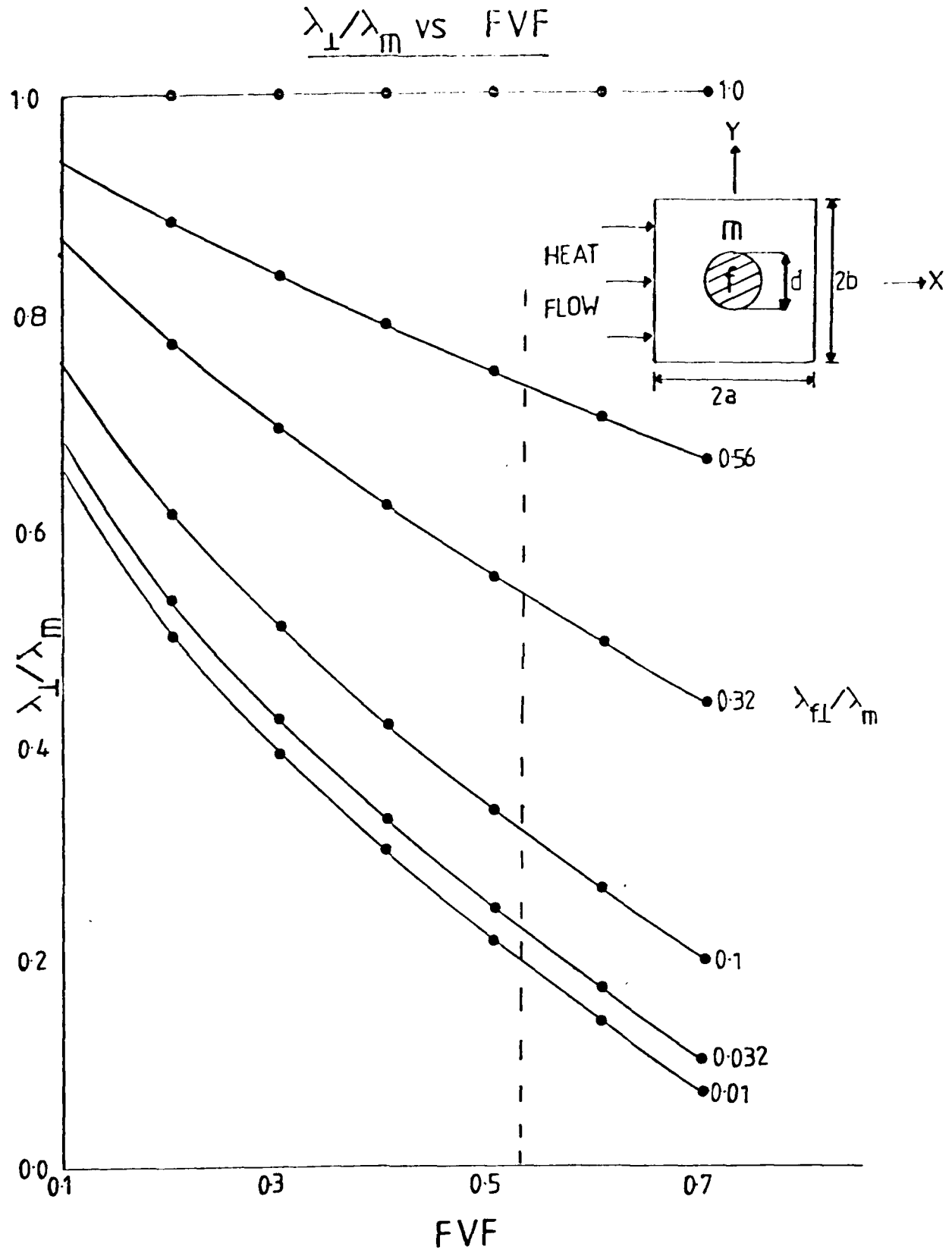
λ⊥/λm vs FVF
1·0
0·8
0·6
0·4
0·2
0·0
λ⊥/λm
0·1
0·3
0·5
0·7
FVF
1·0
0·56
0·32
0·1
0·032
0·01
λf⊥/λm
Y
X
m
f
d
2b
2a
HEAT
FLOW

Figure 38

individual fibres (see Figure 30). The form of the coating varies with fibre type and in the case of fibre 'F' is isotropic[15,16,17]. Where fibres are closely packed (separation less than $1\frac{1}{2}$ fibre diameters) the inter-fibre space may be entirely filled with CVD material[6].

3) The elastic modulus, thermal conductivity and bulk density of CVD CFCC are lower than when CVD is absent. The CVD process tends to seal off the fine porosity of the fibres, preventing infiltration by the matrix[15,16,17].

4) The matrix crystallites in the vicinity of fibres with isotropic CVD coatings are transversely oriented (TOG) w.r.t. the fibre axes[15]. In other regions e.g. cross-over pockets and where spacing between fibres is large, the matrix is isotropic.

5) Matrix crystallites in the vicinity of non CVD'd 'F' fibres are parallel oriented (POG) with the fibre axes[16].

It is clear that the properties of CFCC materials result from a complex interaction of the individual phases. In the case of non CVD'd yarns, the matrix must not only increase fibre conductivity by infill of fibre defects, but also with its POG structure contribute very significantly to axial conductivity.

In the case of CVD'd material, it is more likely that CVD infill is the major influence on axial conductivity with that of the matrix less prominent. In both examples however the matrix properties themselves will be influenced by FVF since this is a factor in determining the proportions of POG/TOG and isotropic matrix.

It may be concluded that, with the present state of knowledge, the modelling of CFCC properties can only succeed if the problems of quantifying the influence of processing can be avoided. This is possible if the 3-D CFCC is considered to be a two phase material comprising

1) Processed fibre yarns, representing the axial reinforcement and

2) isotropic matrix pockets filling the rest of the space in the unit cell geometry. The data required is then simply the thermal properties of a 1-D

composite with appropriate FVF, and the bulk matrix.

(i) CFCC 'A'

The method rests on the assumption that the yarns and matrix pockets are arranged either in series or in parallel and that the resulting thermal model is analogous to series and parallel connected electrical circuits. Essentially, it extends the method used by Knappe and Martinez-Freire[18] to three dimensions.

Along the axis under consideration, the composite unit cell is subdivided into four parallel conduction channels (see Figure 39). It is then required that:

a) The temperature difference ΔT along the heat flow direction is constant.

b) The total heat flow Q may be divided into four parts i.e.

$$Q = Q_1 + Q_2 + Q_3 + Q_4 \tag{6}$$

The thermal conductivity of each channel is calculated using an Ohm's law approach. Thus, for the Z axis channels indicated in Figure 39:

$$\frac{2a}{\lambda_{1Z}} = \frac{s}{\lambda_m} + \frac{2a-s}{\lambda_{\perp x}} \tag{7}$$

giving

$$\lambda_{1Z} = \frac{2a\lambda_m\lambda_{\perp x}}{(s\lambda_{\perp x} + g\lambda_m)} \tag{8}$$

where $\lambda_{\perp x}$ is the transverse conductivity of the X axis yarn.

Similarly,

$$\lambda_{2Z} = \frac{2a\lambda_{\perp x}\lambda_{\perp y}}{(s\lambda_{\perp x} + g\lambda_{\perp y})} \tag{9}$$

$$\lambda_{3Z} = \frac{2a\lambda_m\lambda_{\perp y}}{(s\lambda_m + g\lambda_{\perp y})} \tag{10}$$

Lastly,

$$\lambda_{4Z} = \lambda_{//Z} \tag{11}$$

where $\lambda_{//Z}$ is the parallel conductivity of the Z axis yarn.

The conductivities of the individual channels are then area-weighted and added to obtain the total conductivity of the unit cell. For the Z axis, the following result is obtained:

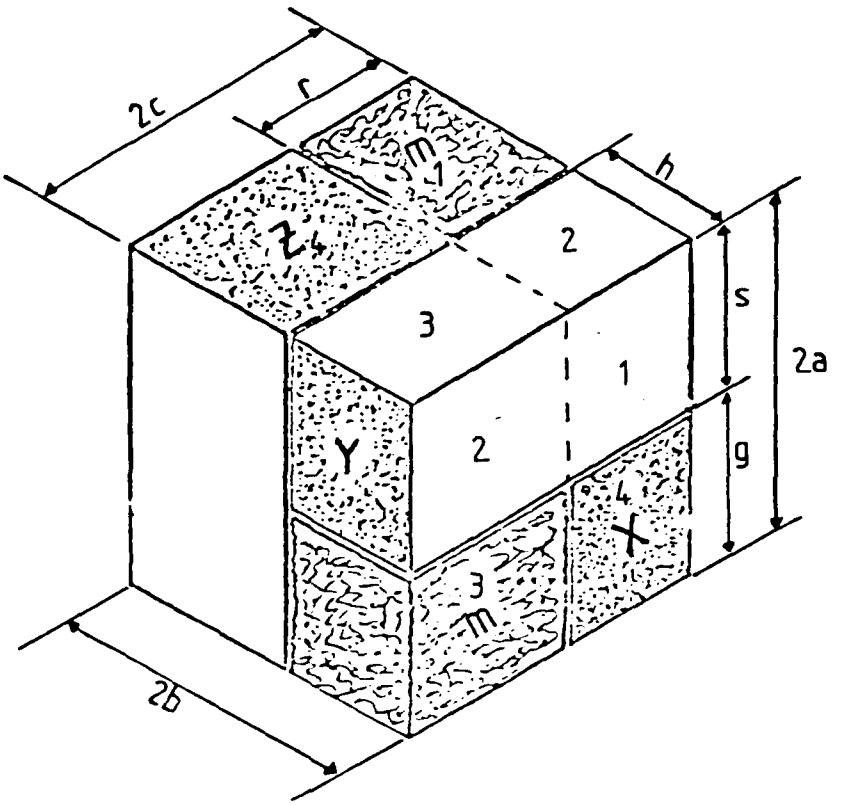

Figure 39

$$\lambda_Z = \frac{\lambda_{1Z}(2b-h)r + \lambda_{2Z}hr + \lambda_{3Z}(2c-r)h + \lambda_{4Z}(2c-r)(2b-h)}{4bc} \qquad (12)$$

And for the X axis:

$$\lambda_X = \frac{\lambda_{1X}rs + \lambda_{2X}(2c-r)s + \lambda_{3X}(2c-r)g + \lambda_{4X}rg}{4ac} \qquad (13)$$

where $\lambda_{1X} = \dfrac{2b\lambda_m\lambda_{\perp Y}}{[h\lambda_m + (2b-h)\lambda_{\perp Y}]}$, $\lambda_{2X} = \dfrac{2b\lambda_{\perp Z}\lambda_{\perp Y}}{[h\lambda_{\perp Z} + (2b-h)\lambda_{\perp Y}]}$

$\lambda_{3X} = \dfrac{2b\lambda_{\perp Z}\lambda_m}{[h\lambda_{\perp Z} + (2b-h)\lambda_m]}$, $\lambda_{4X} = \lambda_{//X}$

In the real composite, these results must represent only the upper bound of channel and unit cell conductivities. Account must also be taken of the effect of structural defects i.e. split yarns, broken interfaces and porosity, though the latter may already be adequately represented within the 1-D composite and bulk matrix data.

For split yarns and broken interfaces perpendicular to heat flow, the lower bound to individual channel conductivity will be zero and from this the unit cell lower bound for the particular defect type can be found. A value between the bounds can then be determined from the frequency with which the defect appears in the composite structure.

(ii) CFCC 'B'

Kessler[14] has derived expressions for the conductivity parallel and perpendicular to the weave of a 2-D CFCC, using a method due to Bruggeman. However, this approach uses the separately measured properties of the individual fibres and matrix. Our investigation shows that these properties are considerably affected by the CVD process and fiber bundle densification.

Analyses of 2-D woven composites have agreed the weave structure has little influence on the conductivity perpendicular to the reinforcement plane[14,18]. Although the non orthogonal FWPF construction increases conduction path length, this is balanced by increased conductivity[14].

Figure 36 has shown that the X-Y weave is not significantly distorted by the Z axis yarns. It seems appropriate, therefore, to retain the orthogonal unit cell analysis for the Z axis conductivity of CFCC 'B'.

The case of the parallel or in-plane (X axis) conductivity is more complex. The weave also results in increased in-plane conductivity paths, but Kessler[14] has estimated that the effect is negligible for the particular weave used in CFCC 'B' (eight-harness satin weave). Figures 34 and 35 have shown the absence of clearly defined matrix cross-over pockets in the X-Y weave, the yarns tending to fill the whole volume available.

The reduced incidence of the relatively high porosity matrix pockets may explain the higher density of CFCC 'B'. Given that the yarn axial conductivity is considerably greater than that of the bulk matrix, the orthogonal analysis must represent a lower bound to the X axis conductivity of this composite.

A simple upper bound can be determined from the assumption that the heat flow paths within the X-Y weave are confined to the X axis yarns. The low conductivity transverse paths through the Y axis yarns are then effectively 'short circuited'. Using the orthogonal analysis, this may be implemented by explanding the X axis yarn into the volume normally occupied by the Y yarn-matrix conduction channel. Although this implies a reduction in yarn FVF, because of processing complications it is not clear that there must be a concomitant reduction in yarn conductivity such as would be implied by Equation 4. Equation 13 then becomes:

$$\lambda_X = \frac{\lambda_{2X}(2c-r)s + \lambda_{3X}(2c-r)g + 2\lambda_{4X}ar}{4ac} \qquad (14)$$

C) 1-D CFCC Properties

It remains merely to establish the compositional similarity of the 1-D composite and the 3-D yarns. The yarn FVF is calculated from the cross-sectional area, the number of filaments/yarn and the effective filament area. This yields FVF of approximately 0.60-0.64[6] which is higher than the FVF of the 1-D composite (0.53).

More importantly however, recent information from AFML has revealed that the 1-D composite was not CVD'd prior to densification and graphitisation. The summary of the influence of processing shows that this will result in significant differences in properties. In particular, it follows from 4) and 5) that CVD'd composites have a lower anisotropy[15]. It seems reasonable to conclude therefore, that the parallel conductivity of the 1-D composite is higher than that of a comparable yarn bundle that has had CVD impregnation whereas the transverse conductivity is lower.

Since no experimental information is available to quantify the influence of CVD on fibre 'F' composites, any attempt to determine the conductivity of a CVD'd yarn from the 1-D composite data can have doubtful merit only. However, since there are no 1-D composites with fibre 'F', CVD and standard process available[6], there is little choice.

Kalnin[11] has demonstrated an empirical linear relationship between fibre thermal conductivity and elastic modulus and Gebhardt[15] reports a 22% decrease in the moduli of CVD'd 1-D composites containing polyacrilonitrile (PAN) fibres. These latter composites generally retain a higher degree of anisotropy after processing with CVD than is found in the equivalent fibre 'F' composites[15]. It seems likely therefore that the decrease in modulus and conductivity of the CVD'd fibre 'F' composite would be greater than 22%.

No quantitative information as to the CVD influence on transverse composite properties is available for fibres of any type. However, it seems clear that the change of orientation from POG to TOG must increase matrix

transverse conductivity very considerably. It seems reasonable to assure also that the transverse conductivity of TOG matrix is higher than the transverse fibre conductivity in which case, the latter will tend to predominate. For example, Figure 38 shows that a 100% increase in matrix transverse conductivity will result in only a 35% increase in transverse conductivity of a composite with similar FVF.

On the basis of the foregoing discussion, the 1-D composite conductivity data is modified in the following way for use in the 3-D composite model.

a) Axial conductivity reduced by a factor of 0.66.

b) Transverse conductivity increased by a factor of 2.0.

No additional correction has been made for the difference in FVF noted earlier. The bulk matrix is used unmodified as its porosity is of a similar order to that of the cross-over pockets[6].

D) Modelling Results

The appropriate unit cell constants are given in Table 4.

The predicted upper and lower bounds of CFCC 'A' X axis conductivity are shown in Tables 5 and 6 together with the experimental data as defined by the least squares function. The rms errors are 27% and 11% respectively. Clearly the lower bound, representing the case of one broken yarn/yarn interface per unit cell, provides the best fit with the experimental data. It was apparent from the microstructural investigation (see Figures 27 and 28) that the lower bound assumptions more closely reflected the real material.

The predicted upper and lower bounds of the CFCC 'A' Z axis are shown in Tables 7 and 8. The rms errors are 12% and 9% respectively. The results are very similar to those of the X axis with the greatest error, in the case of the lower bound, occurring at the extremes of the temperature range.

The predicted conductivity of CFCC 'B' X axis is shown in Tables 9 and 10.

Composite Type	Unit Cell Dimensions mm						
	a	b	c	g	h	r	s
'A'	0.42	0.38	0.38	0.42	0.32	0.32	0.42
'B'	0.127	0.625	0.625	0.127	0.71	0.71	0.127

Table 4

Unit Cell Constants

THERMAL CONDUCTIVITY MODELING OF GRCC A
A X AXIS
UPPER BOUND

TEMPERATURE (K)	EXP. DATA	CAL. DATA	%ERROR
300.0	.643	.943	46.5
350.0	.636	.922	45.1
400.0	.627	.902	43.7
450.0	.619	.881	42.4
500.0	.610	.861	41.1
550.0	.600	.840	39.9
600.0	.591	.819	38.7
650.0	.581	.799	37.5
700.0	.571	.779	36.4
750.0	.561	.759	35.3
800.0	.552	.740	34.2
850.0	.542	.721	33.1
900.0	.532	.703	32.1
950.0	.522	.685	31.1
1000.0	.513	.668	30.1
1050.0	.504	.651	29.2
1100.0	.495	.635	28.3
1150.0	.486	.619	27.4
1200.0	.478	.605	26.6
1250.0	.470	.590	25.7
1300.0	.462	.577	24.9
1350.0	.455	.564	24.2
1400.0	.448	.552	23.4
1450.0	.441	.541	22.7
1500.0	.435	.530	22.0
1550.0	.429	.520	21.3
1600.0	.424	.511	20.6
1650.0	.419	.502	19.9
1700.0	.415	.494	19.2
1750.0	.411	.487	18.5
1800.0	.407	.480	17.8
1850.0	.404	.473	17.2
1900.0	.401	.467	16.4
1950.0	.399	.461	15.7
2000.0	.397	.456	14.9
2050.0	.395	.451	14.1
2100.0	.394	.446	13.3
2150.0	.393	.441	12.4
2200.0	.392	.437	11.4
2250.0	.392	.432	10.3
2300.0	.391	.427	9.2
2350.0	.391	.422	8.0
2400.0	.391	.417	6.6
2450.0	.391	.411	5.2
2500.0	.391	.405	3.6

RMS ERROR= 27.0

Table 5

THERMAL CONDUCTIVITY MODELING OF CFCC A
A X AXIS
LOWER BOUND

TEMPERATURE (K)	EXP. DATA	CAL. DATA	%ERROR
300.0	.643	.779	21.1
350.0	.636	.760	19.5
400.0	.627	.741	18.1
450.0	.619	.722	16.7
500.0	.610	.703	15.4
550.0	.600	.685	14.1
600.0	.591	.667	12.9
650.0	.581	.649	11.7
700.0	.571	.632	10.6
750.0	.561	.615	9.5
800.0	.552	.598	8.5
850.0	.542	.582	7.5
900.0	.532	.567	6.5
950.0	.522	.552	5.6
1000.0	.513	.537	4.7
1050.0	.504	.523	3.8
1100.0	.495	.510	3.0
1150.0	.486	.497	2.2
1200.0	.478	.484	1.4
1250.0	.470	.473	.7
1300.0	.462	.462	-.1
1350.0	.455	.451	-.8
1400.0	.448	.441	-1.5
1450.0	.441	.431	-2.2
1500.0	.435	.422	-2.9
1550.0	.429	.414	-3.5
1600.0	.424	.406	-4.2
1650.0	.419	.399	-4.8
1700.0	.415	.392	-5.5
1750.0	.411	.385	-6.1
1800.0	.407	.379	-6.8
1850.0	.404	.374	-7.5
1900.0	.401	.368	-8.2
1950.0	.399	.363	-8.9
2000.0	.397	.359	-9.6
2050.0	.395	.354	-10.4
2100.0	.394	.350	-11.2
2150.0	.393	.346	-12.0
2200.0	.392	.342	-12.8
2250.0	.392	.338	-13.7
2300.0	.391	.334	-14.7
2350.0	.391	.330	-15.7
2400.0	.391	.325	-16.8
2450.0	.391	.321	-18.0
2500.0	.391	.316	-19.2

RMS ERROR= 10.8

Table 6

[illegible] TIVITY [illegible]
A Z -XIS
UPPER BOUND

TEMPERATURE (K)	EXP. DATA	CAL. DATA	%ERROR
300.0	.934	1.184	26.8
350.0	.916	1.153	25.9
400.0	.899	1.123	24.9
450.0	.882	1.093	23.9
500.0	.866	1.064	22.9
550.0	.849	1.035	21.9
600.0	.833	1.007	20.8
650.0	.818	.980	19.8
700.0	.803	.953	18.7
750.0	.788	.927	17.6
800.0	.773	.902	16.6
850.0	.759	.877	15.5
900.0	.745	.854	14.5
950.0	.732	.831	13.5
1000.0	.719	.809	12.5
1050.0	.706	.788	11.6
1100.0	.694	.768	10.7
1150.0	.682	.748	9.8
1200.0	.670	.730	9.0
1250.0	.659	.712	8.2
1300.0	.648	.696	7.4
1350.0	.637	.680	6.7
1400.0	.627	.665	6.1
1450.0	.617	.651	5.5
1500.0	.607	.638	5.0
1550.0	.598	.625	4.5
1600.0	.590	.613	4.0
1650.0	.581	.602	3.6
1700.0	.573	.592	3.2
1750.0	.566	.582	2.9
1800.0	.558	.573	2.6
1850.0	.552	.564	2.3
1900.0	.545	.556	2.1
1950.0	.539	.549	1.8
2000.0	.533	.541	1.5
2050.0	.528	.534	1.2
2100.0	.523	.528	.9
2150.0	.518	.521	.6
2200.0	.514	.515	.2
2250.0	.511	.509	-.3
2300.0	.507	.503	-.9
2350.0	.504	.496	-1.6
2400.0	.502	.490	-2.4
2450.0	.499	.483	-3.3
2500.0	.498	.476	-4.4

RMS ERROR= 12.4

Table 7

THERMAL CONDUCTIVITY MODELING OF [illegible]
A Z AXIS
LOWER BOUND

TEMPERATURE (K)	EXP. DATA	CAL. DATA	%ERROR
300.0	.934	1.092	16.9
350.0	.916	1.062	15.9
400.0	.899	1.032	14.8
450.0	.882	1.004	13.8
500.0	.866	.975	12.7
550.0	.849	.948	11.6
600.0	.833	.921	10.5
650.0	.818	.895	9.5
700.0	.803	.870	8.4
750.0	.788	.846	7.3
800.0	.773	.822	6.3
850.0	.759	.799	5.3
900.0	.745	.777	4.3
950.0	.732	.756	3.3
1000.0	.719	.736	2.3
1050.0	.706	.716	1.4
1100.0	.694	.697	.5
1150.0	.682	.680	-.3
1200.0	.670	.662	-1.1
1250.0	.659	.646	-1.9
1300.0	.648	.631	-2.6
1350.0	.637	.616	-3.3
1400.0	.627	.602	-3.9
1450.0	.617	.589	-4.5
1500.0	.607	.577	-5.0
1550.0	.598	.565	-5.5
1600.0	.590	.554	-6.0
1650.0	.581	.544	-6.4
1700.0	.573	.534	-6.8
1750.0	.566	.525	-7.2
1800.0	.558	.516	-7.5
1850.0	.552	.508	-7.8
1900.0	.545	.501	-8.1
1950.0	.539	.493	-8.4
2000.0	.533	.487	-8.7
2050.0	.528	.480	-9.1
2100.0	.523	.474	-9.4
2150.0	.518	.468	-9.8
2200.0	.514	.462	-10.2
2250.0	.511	.456	-10.7
2300.0	.507	.450	-11.3
2350.0	.504	.444	-11.9
2400.0	.502	.438	-12.6
2450.0	.499	.432	-13.5
2500.0	.498	.426	-14.5

RMS ERROR= 8.9

Table 8

THERMAL CONDUCTIVITY MODELING OF CFCC B
B X AXIS
UPPER BOUND

TEMPERATURE (K)	EXP. DATA	CAL. DATA	%ERROR
300.0	1.383	1.529	10.5
350.0	1.332	1.483	11.4
400.0	1.283	1.438	12.1
450.0	1.237	1.395	12.8
500.0	1.194	1.354	13.4
550.0	1.153	1.313	13.9
600.0	1.115	1.274	14.3
650.0	1.079	1.237	14.6
700.0	1.045	1.201	14.9
750.0	1.014	1.166	15.0
800.0	.984	1.132	15.1
850.0	.957	1.100	15.0
900.0	.931	1.070	14.9
950.0	.907	1.040	14.7
1000.0	.884	1.012	14.4
1050.0	.863	.985	14.1
1100.0	.844	.959	13.7
1150.0	.825	.935	13.2
1200.0	.808	.911	12.7
1250.0	.793	.889	12.2
1300.0	.778	.868	11.6
1350.0	.764	.848	10.9
1400.0	.752	.829	10.3
1450.0	.740	.811	9.6
1500.0	.729	.794	8.9
1550.0	.719	.778	8.2
1600.0	.710	.763	7.5
1650.0	.701	.749	6.8
1700.0	.693	.735	6.2
1750.0	.685	.723	5.5
1800.0	.678	.711	4.8
1850.0	.671	.699	4.2
1900.0	.664	.688	3.6
1950.0	.658	.678	3.0
2000.0	.653	.668	2.4
2050.0	.647	.659	1.8
2100.0	.642	.650	1.2
2150.0	.637	.641	.7
2200.0	.632	.632	.1
2250.0	.627	.624	-.4
2300.0	.622	.616	-1.0
2350.0	.617	.607	-1.6
2400.0	.612	.599	-2.2
2450.0	.608	.590	-2.9
2500.0	.603	.581	-3.6

RMS ERROR= 10.1

Table 9

T[illegible] . [illegible]TIVITY MODELING OF [illegible]
[illegible] A [illegible]
[illegible]

TEMPERATURE (K)	EXP. DATA	CAL. DATA	%ERROR
300.0	1.383	1.082	-21.8
350.0	1.332	1.055	-20.7
400.0	1.283	1.029	-19.8
450.0	1.237	1.003	-18.9
500.0	1.194	.978	-18.1
550.0	1.153	.952	-17.4
600.0	1.115	.927	-16.8
650.0	1.079	.903	-16.3
700.0	1.045	.879	-15.9
750.0	1.014	.856	-15.6
800.0	.984	.833	-15.4
850.0	.957	.811	-15.2
900.0	.931	.790	-15.2
950.0	.907	.769	-15.2
1000.0	.884	.749	-15.3
1050.0	.863	.730	-15.5
1100.0	.844	.711	-15.7
1150.0	.825	.694	-16.0
1200.0	.808	.677	-16.3
1250.0	.793	.661	-16.7
1300.0	.778	.645	-17.1
1350.0	.764	.631	-17.5
1400.0	.752	.617	-17.9
1450.0	.740	.604	-18.4
1500.0	.729	.592	-18.8
1550.0	.719	.581	-19.3
1600.0	.710	.570	-19.7
1650.0	.701	.560	-20.1
1700.0	.693	.550	-20.5
1750.0	.685	.542	-20.9
1800.0	.678	.533	-21.3
1850.0	.671	.526	-21.7
1900.0	.664	.518	-22.0
1950.0	.658	.512	-22.3
2000.0	.653	.505	-22.6
2050.0	.647	.499	-22.9
2100.0	.642	.493	-23.2
2150.0	.637	.487	-23.4
2200.0	.632	.482	-23.7
2250.0	.627	.476	-24.0
2300.0	.622	.471	-24.3
2350.0	.617	.465	-24.7
2400.0	.612	.459	-25.1
2450.0	.608	.452	-25.6
2500.0	.603	.446	-26.1

RMS ERROR= 19.9

Table 10

As discussed earlier, the upper and lower bounds of this material are different from those of CFCC 'A'. The rms errors are 10% and 20% respectively.

As expected the lower bound, which represents the orthogonal unit cell geometry, consistently underestimates the X axis conductivity. The upper bound, which though exaggerating the weave influence, is in much closer agreement with the experimental data.

Finally, the calculated upper and lower bounds of CFCC 'B' Z axis conductivity are shown in Tables 11 and 12. The rms errors are 24% and 14% respectively. The lower bound chosen is again that of one broken yarn/yarn interface per unit cell and this seems reasonable in view of the evidence provided by the microstructural investigation (see Figures 34 and 35).

9. CONCLUSIONS

It is evident that the modelling of CFCC properties cannot proceed on the basis of the properties of the individual constituent phases. It has not been possible to rigorously test the present CFCC model because of the unavailability of a suitably processed 1-D composite. However, in spite of its basic simplicity and the limitations of the 1-D composite data, the predictions of the CFCC model have shown a reasonable agreement with the experimental data.

With the exception of the X axis of material 'B' which is a special case, CFCC conductivities are reflected more closely by the lower bound solutions. It is believed that the microstructural investigation has shown that these in turn reflect most accurately the structural state of the real composites.

10. FUTURE WORK

In order to gain more accurate information on yarn conductivity, the possibility of machining yarns from the 3-D CFCCs is being investigated.

THERMAL CONDUCTIVITY MODELING OF GRADE A
R Z AXIS
UPPER BOUND

TEMPERATURE (K)	EXP. DATA	CAL. DATA	%ERROR
300.0	.641	.904	41.0
350.0	.633	.885	39.7
400.0	.625	.866	38.5
450.0	.616	.847	37.4
500.0	.607	.828	36.4
550.0	.597	.808	35.4
600.0	.587	.789	34.5
650.0	.576	.770	33.6
700.0	.565	.751	32.8
750.0	.555	.732	32.0
800.0	.544	.714	31.3
850.0	.533	.696	30.6
900.0	.522	.678	29.8
950.0	.512	.661	29.1
1000.0	.502	.645	28.5
1050.0	.492	.629	27.8
1100.0	.483	.613	27.1
1150.0	.474	.598	26.4
1200.0	.465	.584	25.6
1250.0	.457	.571	24.9
1300.0	.449	.558	24.1
1350.0	.442	.546	23.3
1400.0	.436	.534	22.5
1450.0	.430	.523	21.7
1500.0	.425	.513	20.8
1550.0	.420	.503	19.8
1600.0	.416	.494	18.9
1650.0	.413	.486	17.8
1700.0	.410	.474	16.8
1750.0	.407	.471	15.7
1800.0	.406	.465	14.6
1850.0	.404	.458	13.4
1900.0	.404	.453	12.2
1950.0	.403	.447	10.9
2000.0	.403	.442	9.6
2050.0	.404	.437	8.3
2100.0	.405	.433	6.9
2150.0	.406	.428	5.5
2200.0	.407	.424	4.1
2250.0	.409	.419	2.7
2300.0	.410	.415	1.2
2350.0	.412	.410	-.4
2400.0	.413	.405	-1.9
2450.0	.414	.400	-3.5
2500.0	.415	.394	-5.2

RMS ERROR= 24.1

Table 11

THERMAL CONDUCTIVITY MODELING OF [illegible] B
R Z AXIS
LOWER BOUND

TEMPERATURE (K)	EXP. DATA	CAL. DATA	%ERROR
300.0	.641	.720	12.4
350.0	.633	.703	11.0
400.0	.625	.686	9.7
450.0	.616	.668	8.5
500.0	.607	.651	7.4
550.0	.597	.635	6.3
600.0	.587	.618	5.4
650.0	.576	.602	4.5
700.0	.565	.586	3.6
750.0	.555	.570	2.8
800.0	.544	.555	2.1
850.0	.533	.540	1.3
900.0	.522	.526	.6
950.0	.512	.512	-.0
1000.0	.502	.498	-.7
1050.0	.492	.485	-1.4
1100.0	.483	.473	-2.0
1150.0	.474	.461	-2.7
1200.0	.465	.449	-3.3
1250.0	.457	.439	-4.0
1300.0	.449	.428	-4.7
1350.0	.442	.418	-5.4
1400.0	.436	.409	-6.1
1450.0	.430	.400	-6.9
1500.0	.425	.392	-7.7
1550.0	.420	.384	-8.5
1600.0	.416	.377	-9.4
1650.0	.413	.370	-10.3
1700.0	.410	.364	-11.2
1750.0	.407	.358	-12.2
1800.0	.406	.352	-13.2
1850.0	.404	.347	-14.2
1900.0	.404	.342	-15.3
1950.0	.403	.337	-16.4
2000.0	.403	.333	-17.5
2050.0	.404	.329	-18.6
2100.0	.405	.325	-19.7
2150.0	.406	.321	-20.9
2200.0	.407	.317	-22.0
2250.0	.409	.314	-23.2
2300.0	.410	.310	-24.4
2350.0	.412	.306	-25.6
2400.0	.413	.302	-26.8
2450.0	.414	.298	-28.0
2500.0	.415	.294	-29.3

RMS ERROR= 13.6

Table 12

The main problem will be their small size with the consequent risk of damage. If successful, a suitable sample will be made by 'potting' several yarns together in a low conductivity matrix (e.g. epoxy resin or silicon rubber). The major limitation of this approach is that the properties of suitable matrix materials will only allow measurements at low temperatures, necessitating extrapolation for most of the temperature range.

The final stage of the research will be to measure and model the thermal properties of a third CFCC. In this case, a suitable 1-D composite is available which should enable the validity of the present CFCC model to be adequately tested.

References

1. R. Taylor; "Thermal Conductivity of Low Density Carbon", High Temperatures-High Pressures, Vol. 4, 1972, pp. 649-658.

2. H.J. Lee and R.E. Taylor; "Thermophysical Properties of Carbon/Graphite Fibers and MOD-3 Fiber-Reinforced Graphite", Carbon, 1975, Vol. 13, pp. 521-527.

3. R. Taylor and R.N. Procter; AFOSR-TR-79-0065, 1978.

4. R. Taylor and C.M. Fowler; "Thermal Diffusivity of Pure Iron and Dilute Iron Alloys", Proc. XV Thermal Conductivity Conf., Ottawa, Canada, Aug. 24th-26th, 1977.

5. R.E. Taylor and L.M. Clark III; "Finite Pulse Time Effects in Flash Diffusivity Method", High Temperature-High Pressure, Vol. 6, 1974.

6. L.S. Theibert, AFML, Wright-Patterson Air Force Base, Dayton, Ohio, U.S.A.

7. CFCC 'A' Data, Southern Research Institute Report.

8. Private communication, Dr. M. French, Northern Coke Research Laboratory, Newcastle University.

9. Dr. M.L. Minges; AFML-TR-74-96, August 1975.

10. J. Jortner, A.A. Kelton and P.C. Hopkins; "In-Situ Densities of Fiber and Matrices in Carbon-Carbon Composites", MDC G7385, May 1978.

11. I.L. Kalnin; "Thermal Conductivity of High Modulus Carbon Fibres", Composite Reliability, ASTM STP 580, 1975, pp. 560-573.

12. B. Granoff, H.O. Pierson and D.M. Schuster; "Carbon-Felt, Carbon-Matrix Composites: Dependence of Thermal and Mechanical Properties on Fiber Volume Percent", Vol. 7, Materials Technology Series, Technomic Publishing Co., Inc. 1974.

13. G.S. Springer and S.W. Tsai; "Thermal Conductivities of Unidirectional Materials", J. Composite Materials, Vol. 1, 1967, pp. 166-173.

14. Dr. W. Kessler; Report on Carbon Phenolic Composite Thermophysical Properties.

15. J.J. Gebhardt; "Influence of Fiber Coatings on Carbon-Carbon Composite Properties", SAMPE Conference, November 1979, Boston, Massachusetts.

16. E.R. Stover, J.F. D'Andrea, P.N. Bolinger and J.J. Gebhardt; "Development of Interfilament Matrix Structures in CVD Infiltrated Carbon-Carbon", 13th Conference on Carbon, July 18-22, 1977, Irvine, California.

17. J.J. Gebhardt; "Surface Effects in Pyrolytic Infiltration of Carbon Fiber Preforms", 14th Conference on Carbon, June 25-29, 1979, State College, Pennsylvania.

18. K. Maries; "Prediction of Thermal Conductivity of CFF Laminates", CP70/76, Building Research Establishment, Fire Research Station, Hertfordshire, England.